iScience

CellPress
OPEN ACCESS

Article

A specialized population of monocyte-derived tracheal macrophages promote airway epithelial regeneration through a CCR2-dependent mechanism

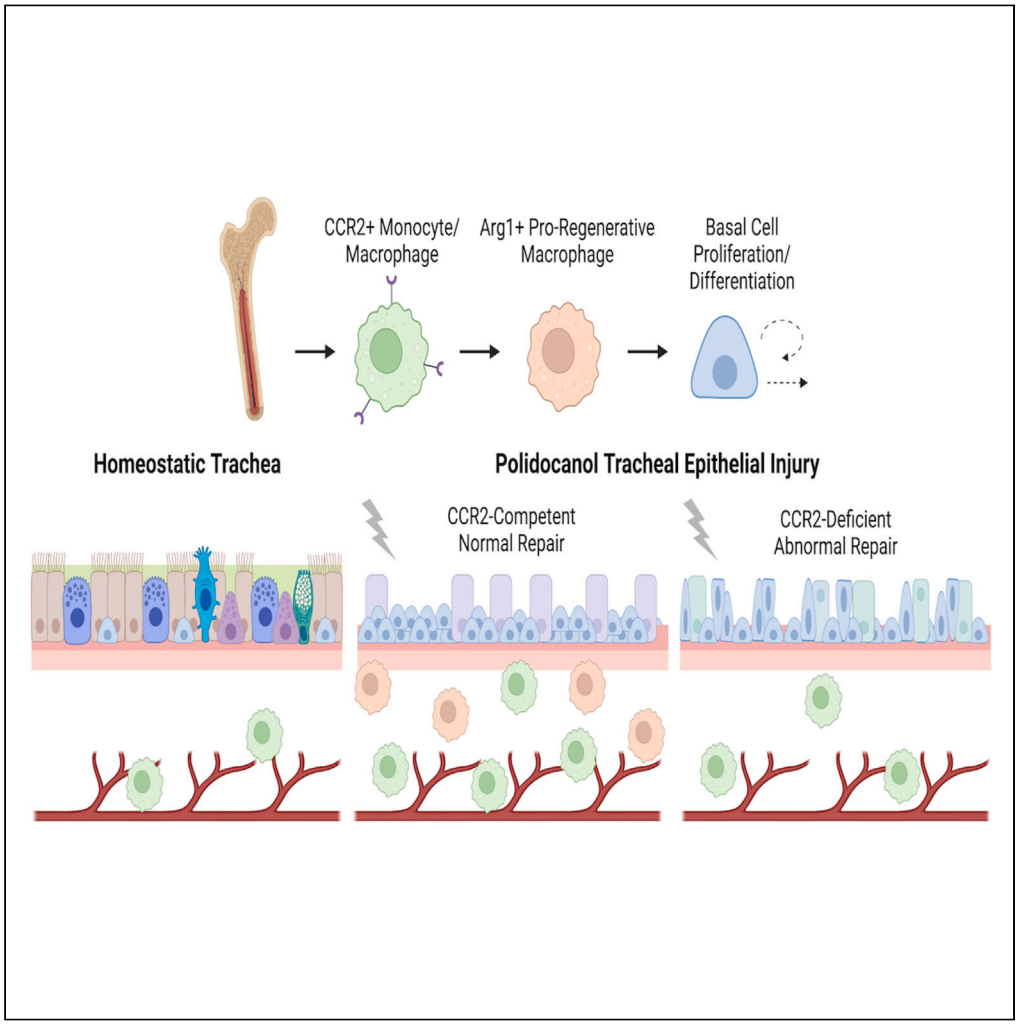

Alexandra B. Ysasi, Anna E. Engler, Pushpinder Singh Bawa, ..., Ruth A. Franklin, Joseph P. Mizgerd, George J. Murphy

gjmurphy@bu.edu

Highlights

Tracheal macrophages are a phenotypically distinct pulmonary macrophage subtype

Murine tracheal macrophages are largely derived via adult hematopoiesis

Monocyte-derived macrophage recruitment is required for normal airway epithelial repair

CCR2 signaling is required for tracheal macrophage function and tissue regeneration

Ysasi et al., iScience 27, 110169
July 19, 2024
https://doi.org/10.1016/j.isci.2024.110169

iScience

CellPress
OPEN ACCESS

Article

A specialized population of monocyte-derived tracheal macrophages promote airway epithelial regeneration through a CCR2-dependent mechanism

Alexandra B. Ysasi,[1,2,3] Anna E. Engler,[1,3,7] Pushpinder Singh Bawa,[1] Feiya Wang,[1] Regan D. Conrad,[4] Anthony K. Yeung,[1,2] Jason R. Rock,[1,3,8] Jennifer Beane-Ebel,[4] Sarah A. Mazzilli,[4] Ruth A. Franklin,[5,6] Joseph P. Mizgerd,[3] and George J. Murphy[1,2,9,*]

SUMMARY

Macrophages are critical for maintenance and repair of mucosal tissues. While functionally distinct subtypes of macrophage are known to have important roles in injury response and repair in the lungs, little is known about macrophages in the proximal conducting airways. Single-cell RNA sequencing and flow cytometry demonstrated murine tracheal macrophages are largely monocyte-derived and are phenotypically distinct from lung macrophages at homeostasis. Following sterile airway injury, monocyte-derived macrophages are recruited to the trachea and activate a pro-regenerative phenotype associated with wound healing. Animals lacking the chemokine receptor CCR2 have reduced numbers of circulating monocytes and tracheal macrophages, deficient pro-regenerative macrophage activation and defective epithelial repair. Together, these studies indicate that recruitment and activation of monocyte-derived tracheal macrophages is CCR2-dependent and is required for normal airway epithelial regeneration.

INTRODUCTION

There has been increasing interest in macrophage heterogeneity and tissue-specific macrophage function in regeneration and repair.[1,2] In the lungs, three main functionally distinct subsets of macrophages have been shown to be important for immune surveillance or tissue maintenance and repair. Alveolar macrophages (AMs) maintain the alveolar spaces by regulating alveolar surfactant, clearing cell debris, and responding to inhaled pathogens.[3,4] Interstitial macrophages (IMs) have been further divided into two distinct subsets based on spatial and functional specialization. LYVE-1^{lo}/MHC-II^{hi}/CX3CR1^{hi} nerve-associated IMs are involved in antigen presentation and immune response and can be phenotypically and spatially distinguished from LYVE-1^{hi}/MHC-II^{lo}/CX3CR1^{lo} blood vessel-associated IMs involved in maintaining vessel integrity and regulating inflammation.[5] Nerve-associated IMs likely overlap with CD206^{lo}/MHC-II^{hi} alveolar-associated IMs that also display features of antigen-presenting cells.[6] CD206^{hi}/MHC-II^{lo} peribronchial IMs were found to be important for regulating tissue homeostasis and were consistent with LYVE-1^{hi}/MHC-II^{lo}/CX3CR1^{lo} blood vessel-associated IMs.[6] This macrophage functional dichotomy between immune response and homeostatic maintenance and repair has been found to be consistent across multiple tissue types, including heart, fat, and skin.[5] Plasticity of macrophage phenotypes has also been observed, with long lasting remodeling of macrophage phenotype in response to pathogen experience,[7,8] tumorigenesis,[9,10] and autoimmune disease.[11]

While functionally distinct subsets of pulmonary macrophages have been identified in the distal lung, relatively little is known about the immune microenvironment in the proximal extrapulmonary airways. With macrophages implicated in the pathogenesis of diseases in the lung and other tissues, a better understanding of macrophage phenotype and function in the airways is critical for understanding and treating human airway diseases including chronic obstructive pulmonary disease (COPD), asthma, and cystic fibrosis.[12–14] We have previously demonstrated that macrophages isolated from the murine trachea at homeostasis possess some broad features of intrapulmonary IMs but are transcriptionally distinct from any macrophage population isolated from the distal lung parenchyma.[15] This work characterized a small subset of tracheal macrophages localized within the pseudostratified epithelium, termed intraepithelial airway macrophages (IAMs), which form close physical connections with airway basal stem cells and are replaced by CCR2^{+} macrophages following epithelial injury. However, the majority

[1]Center for Regenerative Medicine of Boston University and Boston Medical Center, Boston, MA 02118, USA
[2]Section of Hematology and Medical Oncology, Boston University Chobanian & Avedisian School of Medicine, Boston, MA 02118, USA
[3]Pulmonary Center and Department of Medicine, Boston University Chobanian & Avedisian School of Medicine, Boston, MA 02118, USA
[4]Section of Computational Biomedicine, Boston University Chobanian & Avedisian School of Medicine, Boston, MA 02118, USA
[5]Department of Stem Cell and Regenerative Biology, Harvard University, Boston, MA 02115, USA
[6]Department of Immunology, Harvard Medical School, Boston, MA 02115, USA
[7]Present address: Boehringer Ingelheim Pharma Gmbh, Birkendorferstraβe 65, Biberach a.d. Riss 88400, Germany
[8]Present address: Immunology and Regenerative Medicine, Genentech, South San Francisco, CA 94080, USA
[9]Lead contact
*Correspondence: gjmurphy@bu.edu
https://doi.org/10.1016/j.isci.2024.110169

of tracheal macrophages, which are localized in the subepithelial stromal compartment of the airway remain largely uncharacterized. Here, our data suggest that tracheal macrophages are distinct from any previously described pulmonary macrophage subset, most closely resembling peribronchial-associated CD206^{hi}/MHC-II^{lo} tissue maintenance macrophages, but with increased capacity for antigen presentation and immune response. These tracheal macrophages are injury-responsive cells that are rapidly derived from circulating monocytes in a CCR2-dependent manner following airway epithelial injury and are required for efficient repair of the tracheal epithelium.

RESULTS

Murine tracheal macrophages are phenotypically distinct from known pulmonary macrophage subtypes

To characterize tracheal macrophages at the transcriptional level, we performed single cell RNA sequencing (scRNA-seq) on macrophages (live CD45$^+$ F4/80$^+$) isolated from the trachea and distal lung (Figure 1A). Notably, we previously demonstrated that tracheal macrophages are transcriptionally distinct from AMs and IMs isolated from the distal lung (Figure 1B).[16] Reanalysis of these data showed unique expression patterns of known macrophage cell surface markers in tracheal macrophages relative to lung IMs and AMs, including *Siglecf*, *Itgax* (CD11c), *Folr2*, *Cd163*, *Cd36*, *Mrc1* (CD206), *Mertk*, *Itgam* (CD11b), *Cd68*, *Fcgr1* (CD64), *Cd86*, *Cd14*, *Ccr2*, *Siglec1* (CD169), *H2-Ab1* (MHC-II), *Cx3cr1*, and *Lyve1* (Figure 1C).

To expand this transcriptional analysis, we harmonized our scRNA-seq data from tracheal and distal lung CD45$^+$ F4/80$^+$ macrophages with scRNA-seq data from Schyns et al., which analyzed sorted CD45$^+$ F4/80$^+$ CD64$^+$ IMs, as well as Ly6C^{hi} and Ly6C^{lo} monocytes (Figure S1A).[6] Visualization of these two datasets together in a UMAP dimensionality reduction plot revealed macrophages from both experiments cluster close together, while Ly6C^{hi} and Ly6C^{lo} monocytes cluster separately and are more transcriptionally distinct from all macrophage populations (Figures S1B and S1C). Importantly, there is overlap between lung macrophage populations from both datasets, providing an internal control for the harmonization algorithm that was utilized in our analyses. Interestingly, tracheal macrophages in this harmonized data fall mostly within Seurat cluster 3, while distal lung macrophages from both datasets primarily fall within Seurat clusters 0, 1, and 5 (Figures S1C and S1D). Relative to other pulmonary macrophage populations, Seurat cluster 3 that is made up largely of tracheal macrophages displayed increased expression of lysosomal enzymes including γ-interferon-inducible lysosomal thiol reductase (*Ifi30*),[17] scavenger receptors including *Cd163*,[18] and genes relating to anti-inflammatory macrophage function including *Lgals1*.[19,20] This cluster also showed increased expression of genes related to monocyte trafficking including *Ahnak*[21] and regulators of immune response including *Ifi27L2a*,[22] *Lilrb4a*,[23] and *Grn*[24] (Figure S1E).

To complement our transcriptional data, we isolated macrophages (live CD45$^+$ F4/80$^+$) from the trachea and distal lung parenchyma and compared the cell surface protein signature of these populations by multi-parameter flow cytometry (Figure 1A). Tracheal macrophages were CD11b$^+$ CX3CR1$^+$ SiglecF$^-$, similar to distal lung IMs, while also having some features consistent with AMs including being CD80$^+$ CD169$^+$ CD206^{hi}.[25] Tracheal macrophages were also shown to be CD36^{hi} LYVE-1^{hi} CCR2^{hi} CD86^{hi} CD11c^{med} MerTK^{med} CD68^{med}, diverging from expression patterns observed in both AMs and IMs from the distal lung (Figures 1D, S2A, and S2B), with about half of tracheal macrophages also expressing high levels of FOLR2. While several phenotypically distinct IM subtypes have been defined in the distal lung, including CD206^{lo} MHC-II^{hi} alveolar-associated IMs, CD206^{hi} MHC-II^{lo} peribronchial-associated IMs,[6] LYVE-1^{lo} MHC-II^{hi} CX3CR1^{hi} nerve-associated IMs, and LYVE-1^{hi} MHC-II^{lo} CX3CR1^{lo} vessel-associated IMs,[5] tracheal macrophages differed from any known IM subtype by being CD206^{hi} MHC-II^{hi} LYVE-1^{hi} CX3CR1^{hi} (Figure 1E). Experimental replicates for key cell surface markers elevated in tracheal macrophages showed that this phenotypic signature is significantly different from distal lung AMs and IMs and can be reproduced across multiple animals (Figure S2C). These data suggest murine tracheal macrophages differ from any previously characterized pulmonary macrophage subtype, at both the transcript and cell surface protein level.

Previous studies have shown CD206^{hi} peribronchial IMs are functionally specialized toward tissue maintenance and repair processes and have high lysosomal content relative to CD206^{lo} immune responsive IMs.[6] To directly compare differences in macrophage morphology, we sorted tracheal macrophages (live CD45$^+$ F4/80$^+$), CD206^{hi} IMs (CD45$^+$ F4/80$^+$ SiglecF$^-$ CD206$^+$), CD206^{lo} IMs (CD45$^+$ F4/80$^+$ SiglecF$^-$ CD206$^-$), and AMs (CD45$^+$ F4/80$^+$ SiglecF$^+$) and performed cytospins followed by modified Wright-Giemsa staining (Figure 2A). We observed large cytoplasmic vacuoles consistent with macrophage lysosomes in tracheal macrophages that resembled vacuoles visible in some CD206^{hi} IMs (Figure 2B). Flow cytometric analysis showed high levels of intracellular Lamp-1 in tracheal macrophages, as well as in CD206^{hi} IMs and AMs consistent with Lamp-1 levels previously reported in these populations[6] (Figures 2C and 2D). This Lamp-1 staining roughly corresponded to side scatter, with tracheal macrophages having intermediate Lamp-1 and side scatter that was significantly higher than CD206^{lo} IMs but significantly lower than CD206^{hi} IMs (Figures 2C–2E). These results suggest tracheal macrophages have high lysosomal content, consistent with cells involved in endocytosis and tissue maintenance and repair processes.

While CD206^{hi} peribronchial IMs are specialized toward tissue maintenance and repair, CD206^{lo} alveolar-associated IMs and AMs are known to be immune responsive cells that phagocytose and neutralize pathogens. To compare tracheal macrophages to immune responsive distal lung macrophage subtypes, we incubated cells *ex vivo* with *S. aureus* pHrodoRed bioparticles that become fluorescently detectable when internalized into an acidic intracellular environment such as a phagosome. We also measured the inflammatory response to pathogen uptake by quantifying reactive oxygen species (ROS) production using CellROX reagent (Figure 2F). Flow cytometric analysis showed significantly more tracheal macrophages phagocytosed bacterial bioparticles compared to tissue maintenance/repair CD206^{hi} IMs and a similar number of tracheal macrophages phagocytosed bacterial bioparticles compared to immune responsive CD206^{lo} IMs and AMs (Figure 2G). We also observed a significant increase in ROS production in tracheal macrophages that phagocytosed bacterial bioparticles (pHrodoRed+) versus cells that did not (pHrodoRed-), suggesting phagocytosis of these bioparticles initiates metabolic changes and inflammatory

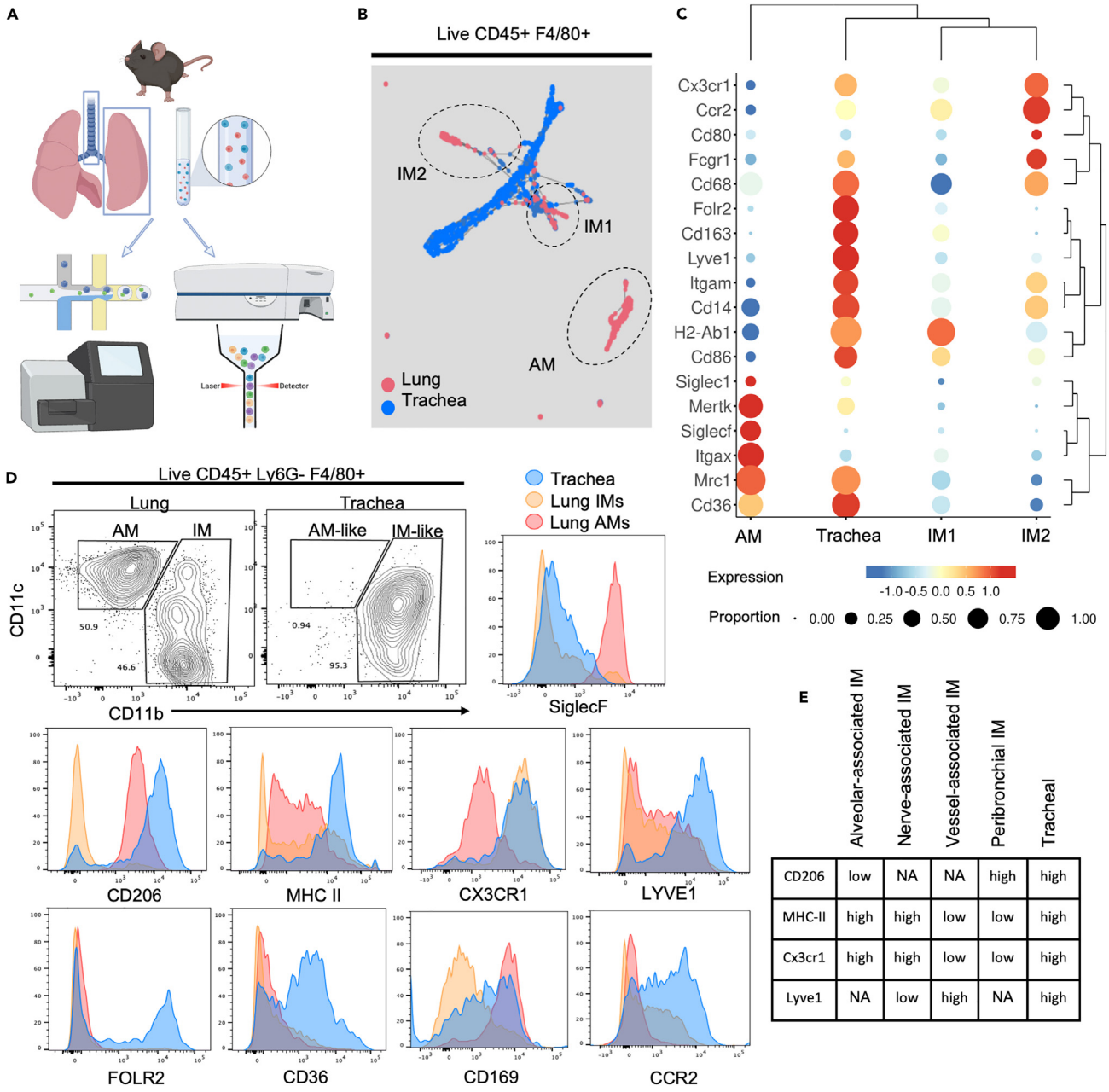

	Alveolar-associated IM	Nerve-associated IM	Vessel-associated IM	Peribronchial IM	Tracheal
CD206	low	NA	NA	high	high
MHC-II	high	high	low	low	high
Cx3cr1	high	high	low	low	high
Lyve1	NA	low	high	NA	high

Figure 1. Murine tracheal macrophages resemble distal lung interstitial macrophages but have a distinct transcriptional and cell surface protein signature

(A) Experimental outline of trachea and lung comparative scRNA-seq and immunophenotyping.

(B) SPRING dimensionality reduction plot of CD45$^+$ F4/80$^+$ macrophages isolated from trachea (1050 cells) and lung (460 cells) (n = 5 per tissue, pooled for sequencing).

(C) Heatmap of selected genes encoding macrophage cell surface markers.

(D) Flow cytometric immunophenotyping of tracheal macrophages relative to lung AMs and IMs (n = 5 per tissue, data pooled in histograms).

(E) Tracheal macrophage surface phenotype relative to previously published distal lung macrophage subtypes (Schyns et al., Nat Comm 2019; Chakarov et al., Science 2019) (NA = not available).

responses in these cells (Figure 2H). AMs are known to efficiently neutralize inhaled pathogens by undergoing apoptosis following bacterial phagocytosis,[26] but significantly fewer tracheal macrophages undergo apoptosis following phagocytosis of bacterial bioparticles (Figure 2I). These data suggest that tracheal macrophages are immune responsive cells that uptake bacterial bioparticles and initiate inflammatory responses to infection, but not to the same degree as AMs that function as front-line responders to inhaled pathogens in the lung.

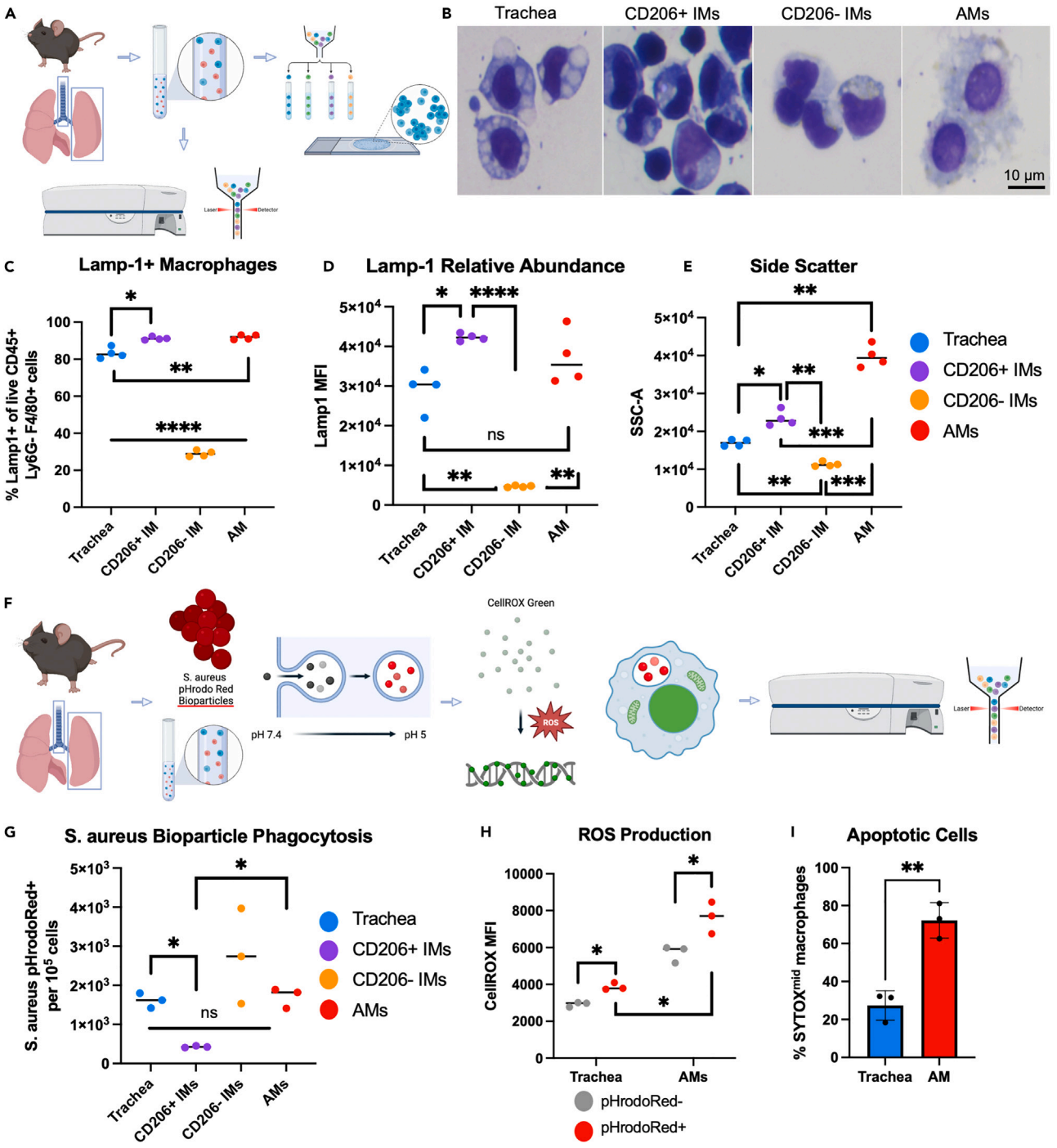

Figure 2. Tracheal macrophages resemble CD206^{hi} peribronchial interstitial macrophages, but with increased capacity for antigen presentation and immune response

(A) Experimental outline of trachea and lung macrophage cytospin and flow cytometric analysis.

(B) Diff-Quik modified Wright-Giemsa histological stain of sorted tracheal macrophages (live CD45$^+$ F4/80$^+$), CD206^{hi}IMs (CD45$^+$ F4/80$^+$ SiglecF$^-$ CD206$^+$), CD206^{lo} IMs (CD45$^+$ F4/80$^+$ SiglecF$^-$ CD206$^-$), and AMs (CD45$^+$ F4/80$^+$ SiglecF$^+$) (n = 4 per tissue) (Scale: 10 μm).

(C) Proportion of cells expressing the intracellular lysosomal marker Lamp1 by flow cytometry (n = 4 per tissue). Data are presented as mean values.

(D) Relative abundance of Lamp1 intracellular protein quantified by mean fluorescent intensity (MFI) (n = 4 per tissue). Data are presented as mean values.

(E) Quantification of macrophage granularity by side scatter (SSC) (n = 4 per tissue). Data are presented as mean values.

(F) Experimental outline of *ex vivo* assays evaluating macrophage phagocytosis and reactive oxygen species (ROS) production.

Figure 2. *Continued*

(G) Relative number of cells phagocytosing pH-sensitive fluorescent bacterial bioparticles (n = 3 per tissue). Data are presented as mean values.

(H) Quantification of ROS production in macrophages that have phagocytosed bacterial bioparticles (pHrodoRed^{+}) versus macrophages that have not taken up bioparticles (pHrodoRed^{-}) (n = 3 per tissue). Data are presented as mean values.

(I) Proportion of apoptotic macrophages (SYTOX^{mid}) following exposure to bacterial bioparticles (n = 3 per tissue). Data are presented as mean ± SD.

*p < 0.05, **p < 0.01, ***p < 0.001, ****p < 0.0001.

Together these results suggest that tracheal macrophages are transcriptionally and phenotypically distinct from any macrophage subtype previously characterized in the distal lung. Tracheal macrophages share features of tissue maintenance/repair and immune responsive macrophage subtypes but has an intermediate phenotype that may suggest these cells are functionally involved in both tissue maintenance/repair and immune surveillance processes in the proximal conducting airways.

Tracheal macrophages are primarily derived from Flk2-dependent adult hematopoiesis

Distal lung macrophage populations are known to be derived from early embryonic waves of hematopoiesis and can persist via self-renewal for approximately one year after birth.[6,27] As the ontogeny of tracheal macrophages has not been previously studied, we sought to characterize the hematopoietic origin and homeostatic proliferation status of tracheal macrophages. Harmonized scRNA-seq data comparing tracheal macrophages to lung IMs and Ly6C$^{hi/lo}$ monocytes (Figure 3A) shows mixed expression of mature macrophage markers and Ly6C$^{hi/lo}$ monocyte markers. Expression of monocyte markers is largely absent from IMs in the distal lung. This suggested that tracheal macrophages are more transcriptionally similar to monocytes than distal lung macrophages, pointing to a possible monocyte developmental lineage.

To evaluate whether tracheal macrophages self-renew at homeostasis, we injected mice with EdU 3 h prior to tissue harvest and quantified the number of actively proliferating macrophages incorporating EdU. Unlike CD206^{hi} peribronchial IMs, which are approximately 60% proliferative,[6] only 0.97% of tracheal macrophages were shown to be actively proliferating at the time of tissue harvest (Figure 3B). As only a minute fraction of tracheal macrophages were found to be undergoing self-renewal at homeostasis at the time of analysis, we next sought to characterize the hematopoietic origin of these cells using transgenic Flk-Switch mice[28] to fluorescently label cells derived from embryonic versus adult hematopoietic processes. In this model, cells ubiquitously express TdTomato (TdTom) at baseline. Flk2 is a receptor tyrosine kinase required for the differentiation of adult hematopoietic stem cells. Cells that activate the *Flk2* promoter undergo Cre-mediated recombination that removes the TdTom reporter construct and permanently drives expression of green fluorescent protein (GFP) in all Flk2^{+} cells and their progeny (Figure 3C).[28] We analyzed homeostatic tracheal macrophages (live extravascular CD45^{+} Ly6G^{-} F4/80^{+}) from mice 8–12 weeks of age and found that at least 80% of tracheal macrophages were GFP^{+}, indicating they are derived from Flk2-dependent adult hematopoietic processes (Figures 3D and 3E). As the vast majority of adult hematopoiesis occurs in the bone marrow, it is likely that GFP^{+} tracheal macrophages are largely bone marrow-derived cells. Furthermore, we confirmed that the monocyte marker Ly6C is present only in the GFP^{+} fraction of analyzed macrophages, consistent with a monocyte-derived population (Figure 3F). The vast majority (at least 90%) of tracheal macrophages are Ly6C^{-} at homeostasis, suggesting only a small subset of these macrophages have recently differentiated from monocytes (Figure 3G).

Analysis of published scRNA-seq data profiling pulmonary macrophage populations in the human lung and extrapulmonary airways shows that this monocyte-derived macrophage phenotype may be conserved across species. Madissoon et al. (2023) were able to generate a spatial atlas of cells in proximal-to-distal regions of healthy human lungs by utilizing rapid sample collection from decreased organ transplant donors.[29] By analyzing the macrophage populations within this dataset, we were able to visualize 9 macrophage subpopulations that were isolated from large conducting airways including the trachea and bronchi and the distal lung parenchyma (Figures S3A and S2B). We observed that human tracheas had a high proportion of CX3CR1+ macrophages (Macro_CX3CR1, 62% in trachea compared with an average of 16% in other locations, p < 0.01; Figures S3A and S3C), consistent with monocyte-derived macrophages found in the mouse respiratory tract. In addition, we generated a gene signature for murine tracheal monocytes using the top 100 DEGs identified in tracheal macrophages relative to other murine tracheal immune populations and found the metagene score for murine tracheal macrophages was most enriched in human macrophages isolated from the trachea (p < 0.001 for all pairwise comparisons between trachea and other locations; Figures S3D and S3E). The murine tracheal macrophage metagene score was also elevated in CX3CR1+ macrophages, chemokine producing macrophages (Macro_CCL), and interstitial macrophages (Macro_interstitial) (p < 0.001 for all cell type pairwise comparisons except non-significant for CX3CR1^{+} vs. interstitial macrophages; Figure S3F). These data suggest that human tracheal macrophages share basic features of the monocyte-derived interstitial macrophages that we describe in the mouse trachea, though additional work is needed to functionally characterize macrophage subpopulations in the human conducting airways relative to the distal lung parenchyma.

Monocyte-derived tracheal macrophages are recruited to the airway following injury

To study how these monocyte-derived tracheal macrophages respond to airway injury, we used a model of polidocanol-induced tracheal epithelial injury, as previously described (Figure 4A). Briefly, polidocanol is administered to anesthetized mice intraorally. A forced inspiration maneuver coats the proximal airway in polidocanol, damaging the luminal portion of the tracheal pseudostratified epithelium. Residual basal stem cells proliferate and differentiate within about 7 days to regenerate the tracheal epithelium.[15]

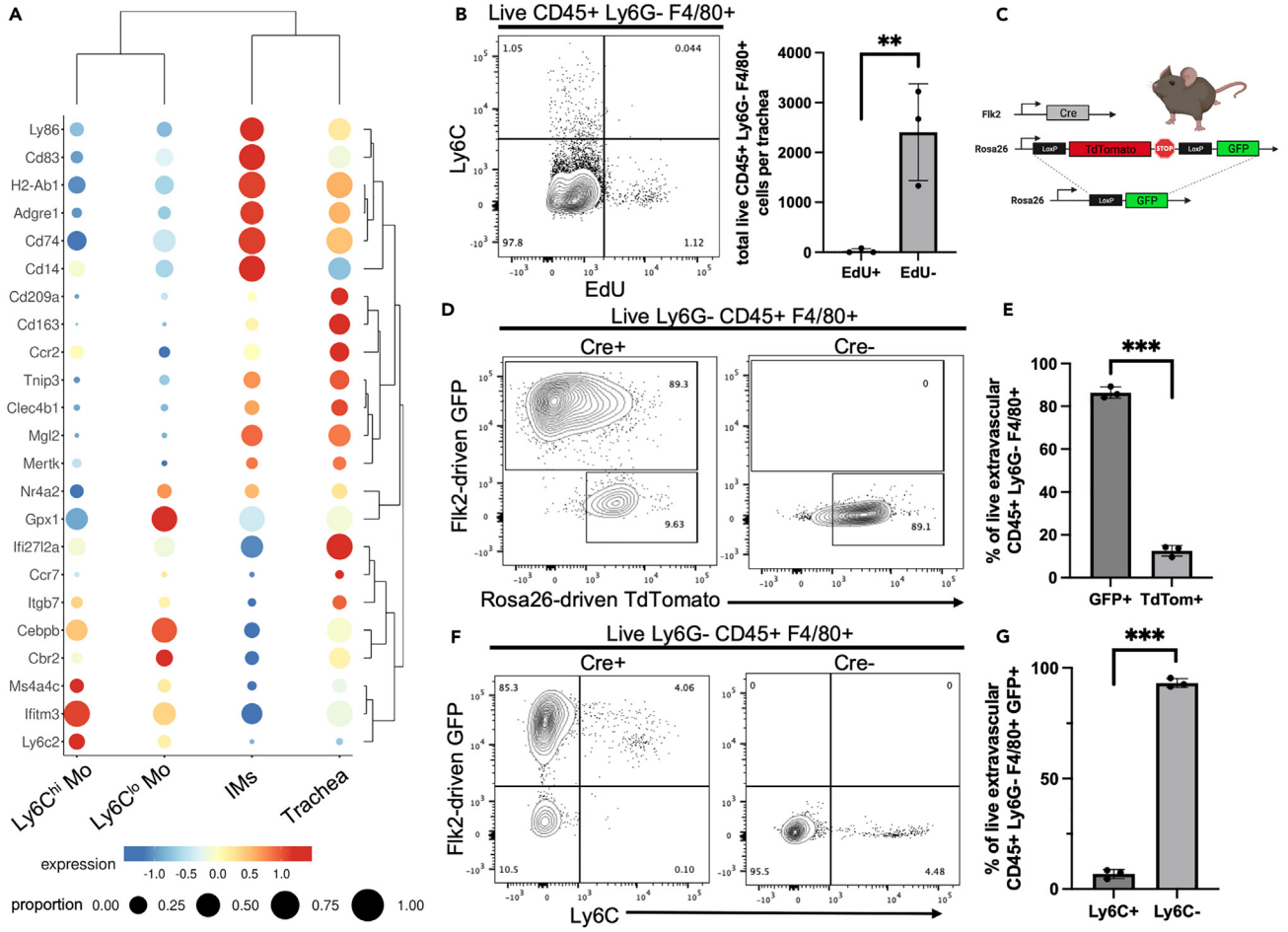

Figure 3. Tracheal macrophages are primarily derived from Flk2-dependent adult hematopoiesis

(A) Bubbleplot of harmonized scRNA-seq data (Figure S1) shows tracheal macrophages express markers of Ly6C^{hi} and Ly6C^{lo} monocytes.

(B) Flow cytometry of wild-type mice shows a lack of tracheal macrophage proliferation (EdU^{+}) at homeostasis (n = 3). Data are presented as mean ± SD.

(C) Transgenic construct of Flk-Switch mice used to quantify macrophage hematopoietic origin.

(D) Flow cytometry in Flk-Switch mice shows tracheal macrophages are largely GFP^{+} indicating Flk2-dependent hematopoietic origin (n = 3).

(E) Quantification of bone marrow derived (GFP^{+}) versus embryonic derived (TdTom^{+}) tracheal macrophages (n = 3). Data are presented as mean ± SD.

(F) Monocyte marker Ly6C is only expressed in GFP^{+} macrophage fraction (n = 3).

(G) Quantification of tracheal macrophages by Ly6C expression (n = 3). Data are presented as mean ± SD.

*p < 0.05, **p < 0.01, ***p < 0.001, ****p < 0.0001.

We first performed polidocanol injury in WT mice to analyze immune cell recruitment and response to airway injury. We observed an increase in the number of immune cells in the trachea within 24 h of polidocanol injury (Figure 4B). This immune cell expansion in the first 24 h after injury is largely due to an influx of neutrophils (live CD45^{+} Ly6G^{+}) (Figure 4D) and monocytes (live CD45^{+} Ly6G^{-} Ly6C^{+}) (Figures 4C and 4E) which quickly returns to near baseline levels by 3 days post-injury. Recruited neutrophils express genes related to phagocytosis, suggesting they may be involved in removal of epithelial cell debris, and lack expression of genes related to degranulation and inflammatory signaling, consistent with a sterile injury response (Figure S4). The peak of monocyte recruitment at day 1 is followed by an increase in the number of tracheal macrophages (Figures 4C and 4F) 3 days after injury, which returns to near baseline levels by 7 days post-injury, consistent with an influx of monocyte-derived macrophages. Notably, there is a minimal proliferation of existing tissue-resident macrophages as identified by EdU incorporation, consistent with recruitment of monocyte-derived cells (Figures 4C and 4G). We also observed an increase in neutrophil production of chemokines and cytokines including Ccl3, Ccrl2, and Csf1 (Figure S4) that may promote monocyte chemotaxis and macrophage differentiation.[30–32]

Analysis of airway injury response in Flk-Switch mice revealed a significant increase in the number of GFP^{+} tracheal macrophages 1 and 3 days post-injury, with at least 80% of tracheal macrophages being GFP^{+} cells derived from Flk2-dependent adult hematopoiesis (Figure 4H). There is a minor but significant increase in the number of TdTom^{+} macrophages 3 days after injury, which corresponds to a detectable but statistically insignificant increase in macrophage proliferation 3 days after injury (Figure 4H). Together these data show that there is a

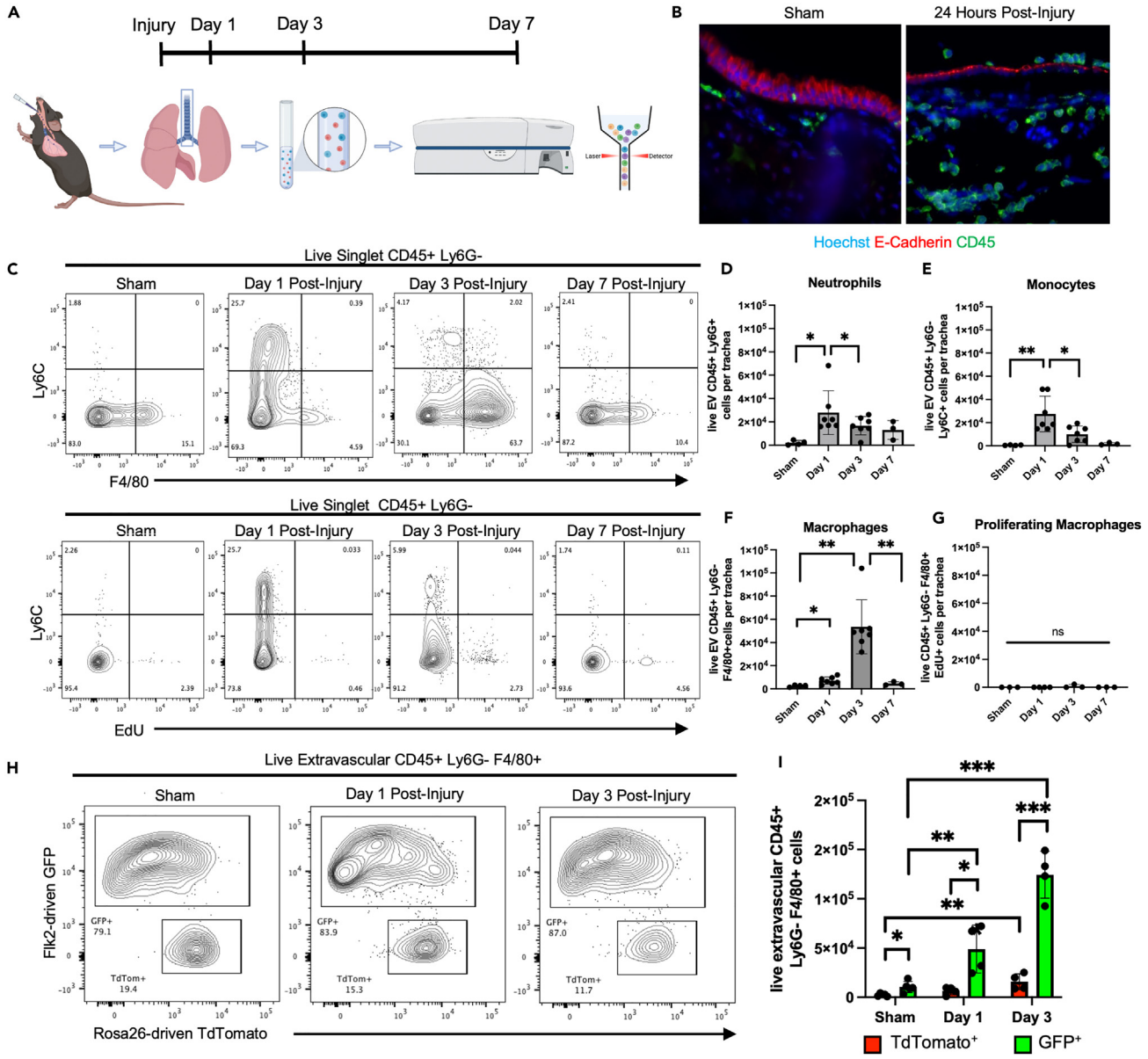

Figure 4. Tracheal macrophages are derived from recruited circulating monocytes following airway injury

(A) Experimental outline for flow cytometry analysis of polidocanol injured airways.

(B) Immunofluorescence (IF) of control and polidocanol injured trachea showing epithelial (E-Cadherin+) injury and immune cell ($CD45^+$) influx.

(C–F) Flow cytometry of WT tracheas 1, 3, and 7 days after polidocanol injury plus sham control. Post-injury quantification of neutrophils ($CD45^+$ $Ly6G^+$) (D), monocytes ($CD45^+$ $Ly6G^-$ $Ly6C^+$) (E), and macrophages ($CD45^+$ $Ly6G^-$ $F4/80^+$) (F) (sham: $n = 4$, day 1: $n = 7$, day 3: $n = 7$, day 7: $n = 3$). Data are presented as mean ± SD.

(G) Quantification of proliferating macrophages ($CD45^+$ $Ly6G^-$ $F4/80^+EdU^+$) (sham: $n = 3$, day 1: $n = 4$, day 3: $n = 3$, day 7: $n = 3$). Data are presented as mean ± SD.

(H and I) Analysis (H) and quantification (I) of post-injury macrophage origin using Flk-Switch mice (all groups: $n = 4$). Data are presented as mean ± SD.

$^*p < 0.05$, $^{**}p < 0.01$, $^{***}p < 0.001$, $^{****}p < 0.0001$.

significant expansion of tracheal macrophages following airway epithelial injury and these cells are largely derived from monocytes generated through Flk2-dependent adult hematopoiesis.

Monocyte-derived tracheal macrophages rapidly adopt an activated pro-regenerative phenotype following airway injury

Further analysis of injury-responsive tracheal macrophages by flow cytometry revealed a significant increase in the expression of the pro-regenerative activation marker Arginase-1 (Arg1) by 3 days post-injury (Figures 5A and 5B), consistent with our previous report.[15] These

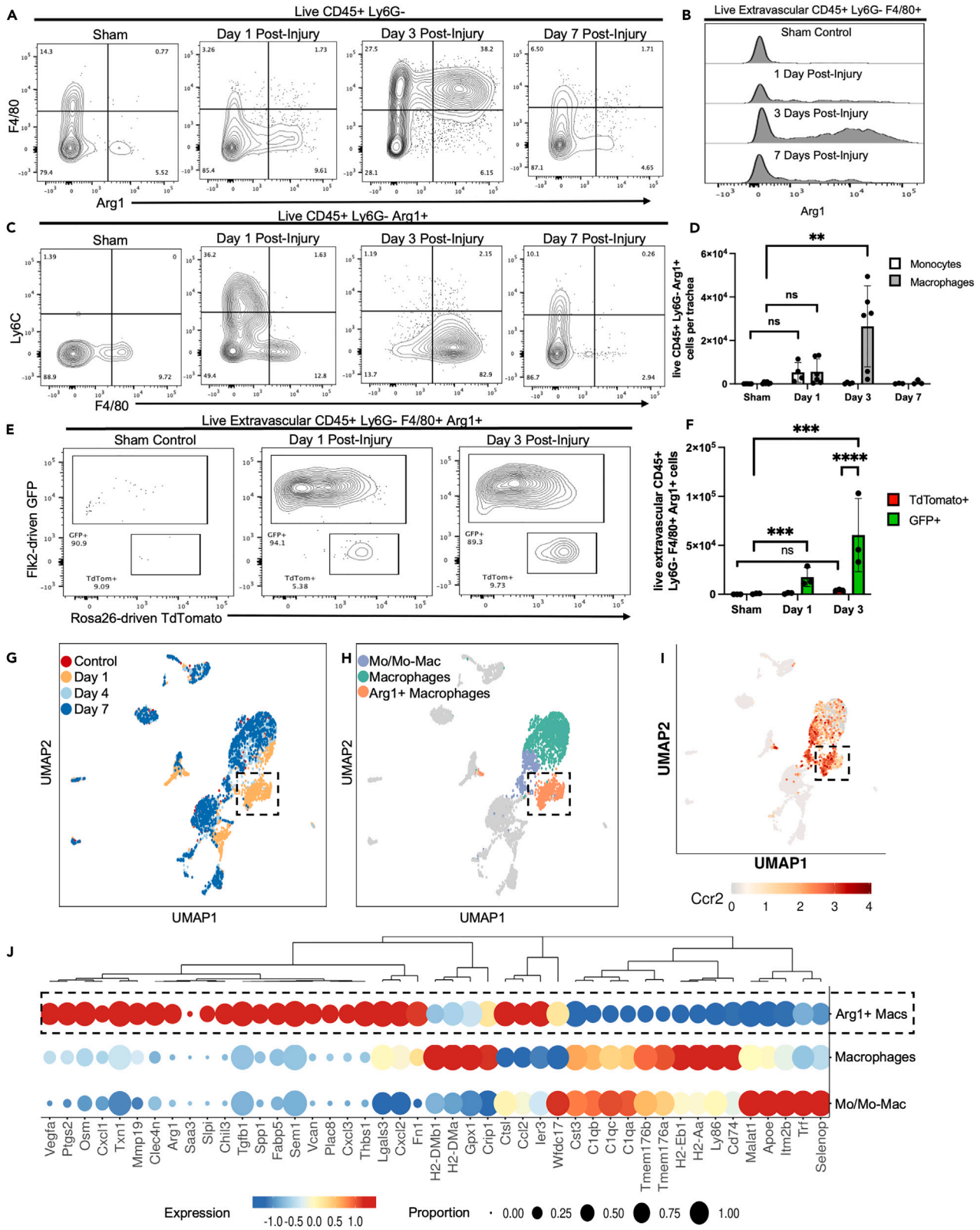
A
Live CD45+ Ly6G-
Sham
Day 1 Post-Injury
Day 3 Post-Injury
Day 7 Post-Injury
F4/80
Arg1
B
Live Extravascular CD45+ Ly6G- F4/80+
Sham Control
1 Day Post-Injury
3 Days Post-Injury
7 Days Post-Injury
Arg1
C
Live CD45+ Ly6G- Arg1+
Ly6C
F4/80
D
live CD45+ Ly6G- Arg1+ cells per trachea
Monocytes
Macrophages
Sham
Day 1
Day 3
Day 7
E
Live Extravascular CD45+ Ly6G- F4/80+ Arg1+
Flk2-driven GFP
Rosa26-driven TdTomato
F
live extravascular CD45+ Ly6G- F4/80+ Arg1+ cells
TdTomato+
GFP+
G
Control
Day 1
Day 4
Day 7
UMAP1
UMAP2
H
Mo/Mo-Mac
Macrophages
Arg1+ Macrophages
I
Ccr2
J
Arg1+ Macs
Macrophages
Mo/Mo-Mac
Vegfa Ptgs2 Osm Cxcl1 Txn1 Mmp19 Clec4n Arg1 Saa3 Slpi Chil3 Tgfb1 Spp1 Fabp5 Sem1 Vcan Plac8 Cxcl3 Thbs1 Lgals3 Cxcl2 Fn1 H2-DMb1 H2-DMa Gpx1 Crip1 Ctsl Ccl2 Ier3 Wfdc17 Cst3 C1qb C1qc C1qa Tmem176b Tmem176a H2-Eb1 H2-Aa Ly86 Cd74 Malat1 Apoe Itm2b Trf Selenop
Expression
Proportion

Figure 5. Monocyte-derived tracheal macrophages efficiently adopt an activated pro-regenerative phenotype after airway injury

(A) Flow cytometry of Arg1$^+$ pro-regenerative macrophages in injured tracheas.

(B) Representative histograms of Arg1 in tracheal macrophages following injury.

(C) Flow cytometry of Arg1$^+$ cells (CD45$^+$ Ly6G$^-$) expressing monocyte (Ly6C$^+$) or mature macrophage (F4/80$^+$) markers.

(D) Quantification of monocyte-like (Ly6C$^+$) (sham: $n = 4$, day 1: $n = 4$, day 3: $n = 4$, day 7: $n = 3$) or mature (F4/80$^+$) Arg1$^+$ macrophages (sham: $n = 6$, day 1: $n = 6$, day 3: n = 6 days 7: $n = 3$) after injury. Data are presented as mean ± SD.

(E) Flow cytometry showing Arg1+ extravascular macrophages (CD45$^+$ Ly6G$^-$ F4/80$^+$) in Flk-Switch mice.

(F) Quantification of Arg1$^+$ tracheal macrophages by hematopoietic origin (all groups: $n = 3$). Data are presented as mean ± SD.

(G) UMAP dimensionality reduction of scRNA-seq data from CD45$^+$ tracheal cells before and after polidocanol injury, displayed by post-injury time point. Dotted line highlights Arg1$^+$ macrophage population ($n = 3$ per condition, pooled for sequencing).

(H) Subsequent analysis limited to monocyte and macrophage populations (2251 cells).

(I) Expression of monocyte marker Ccr2 in Arg1$^+$ macrophage cluster.

(J) Selected DEGs consistent with monocyte (cluster 3, 387 cells), mature macrophage (cluster 0; 1398 cells), and pro-regenerative macrophage (cluster 2; 466 cells) cell identities showing Arg1$^+$ macrophages express growth factors, cytokines, and ECM components associated with wound-healing.

*$p < 0.05$, **$p < 0.01$, ***$p < 0.001$, ****$p < 0.0001$.

Arg1$^+$ activated macrophages are Ly6C$^+$ 1 day after injury at the peak of monocyte recruitment and are overwhelmingly GFP$^+$ in Flk-Switch mice, indicating that these pro-regenerative activated cells are monocyte-derived (Figures 5C–5F).

To profile transcriptional changes in injury-responsive immune cells, we performed scRNA-seq on CD45$^+$ cells 1, 4, and 7 days post-polidocanol tracheal injury, as well as uninjured controls. As previously reported, monocytes and macrophages make up a significant proportion of post-injury immune cells captured for sequencing, with a significant increase in cells with a pro-regenerative gene signature 1 day after injury (Figures 5G and 5H).[15] This cluster expressed known markers of activated "wound healing" macrophages (*Arg1*, *Chil3*) as well as a number of factors that may contribute to remodeling and repair of the airway epithelium including growth factors (*Tgfb1*, *Vegfa*), extracellular matrix enzymes and constituents (*Mmp19*, *Fn1*) and chemokines implicated in wound healing (*Cxcl1*, *Cxcl2*).[33,34] This cluster also expressed markers consistent with anti-inflammatory monocyte-derived "pro-resolving" intestinal macrophages including *Fabp5*, *Plac8*, and *Spp1* (Figure 5J).[35] We have also previously demonstrated that Arg1$^+$ macrophages directly influence basal cell growth *in vitro*.[15] Basal cells cultured in 3-dimensional organoids grow significantly larger when co-cultured with Arg1$^+$ tracheal macrophages compared to basal cells cultured with Arg1$^-$ myeloid cells or without any immune cell co-culture, suggesting these activated macrophages directly promote basal cell expansion.

Interestingly, there was a population of Ly6C$^+$ F4/80$^-$ Arg1$^+$ cells detected by flow cytometry 1 day after injury which transitioned into a Ly6C$^-$ F4/80$^+$ Arg1$^+$ population by 3 days post-injury (Figures 5C and 5D), suggesting recruited monocytes are capable of activating Arg1 expression before fully maturing to F4/80$^+$ macrophages. Consistent with this observation, the pro-regenerative activated macrophage gene signature is primarily present in sequenced myeloid cells 1 day post-injury and this cluster retains expression of monocyte markers including *Ccr2* (Figures 5G–5I). While all cells expressing Arg1 transcript express the gene encoding F4/80 (*Adgre1*), about half of Arg1$^+$ cells by flow cytometry do not yet display F4/80 cell surface protein and have a cell surface phenotype consistent with monocytes or immature macrophages (F4/80$^-$ Ly6C$^+$) (Figures 5C and 5D). These data are consistent with rapid activation of a pro-regenerative transcriptional program in monocyte-derived macrophages that have not yet fully differentiated or matured. Together, these data suggest that monocyte-derived tracheal macrophages are highly injury-responsive cells that are recruited to the injured airway within one day of injury and rapidly activate anti-inflammatory tissue remodeling processes to facilitate epithelial repair.

Mice lacking functional CCR2 have reduced macrophage recruitment and activation

To further understand the mechanisms regulating monocyte-derived macrophage recruitment and activation, we utilized *Ccr2*-RFP reporter/depletion mice. In this model, RFP is knocked into the endogenous *Ccr2* locus, which prevents production of functional CCR2 protein. Heterozygous animals will generate the RFP reporter from one allele, and functional CCR2 protein from the other allele, while homozygous animals will generate an RFP reporter in cells that turn on the *Ccr2* promoter without making functional CCR2 protein (Figures 6A and 6B).[36] Consistent with previous reports,[36–40] homozygote *Ccr2*$^{RFP/RFP}$ animals have significantly reduced numbers of Ly6C^{hi} circulating monocytes at homeostasis (Figure 6C). As the vast majority of tracheal macrophages are monocyte-derived both before and after injury (Figure 4), we also observed a significant reduction in the number of mature F4/80$^+$ tracheal macrophages at homeostasis (Figure 6D).

Following polidocanol injury, the majority of recruited CCR2$^+$ monocytes expressed the mature macrophage marker F4/80 within 3 days of airway injury in heterozygous animals with functional CCR2 protein (Figure 6E). In *Ccr2*$^{RFP/RFP}$ animals lacking functional CCR2, RFP$^+$ cells were able to migrate into the trachea in a reduced capacity following airway injury, but there was a 65% reduction in the number of F4/80$^+$ macrophages in *Ccr2*$^{RFP/RFP}$ animals 3 days after injury (Figures 6G and 6I). This is consistent with previous reports that observe a reduction, but not a total absence of Ly6C^{hi} monocyte egress from bone marrow in CCR2-deficient animals.[36–40] Redundant and context specific roles of other chemokine receptors including CX3CR1 and CCR5 likely allow for the migration of monocytes into peripheral tissues in the absence of CCR2.[41–43] Importantly, there is also a 321% decrease in the number of Arg1$^+$ activated macrophages by 3 days post-injury in *Ccr2*$^{RFP/RFP}$ mice compared to heterozygous controls (Figures 6F and 6H). We observed minor but statistically significant expansion of the F4/80$^+$ macrophage population in CCR2-deficient animals by 3 days post-injury, with Arg1 expression present in a reduced proportion of this population (Figures 6F–6H). This suggests that while the CCR2 signaling axis is important for normal recruitment, maturation, and activation of monocyte-derived macrophages

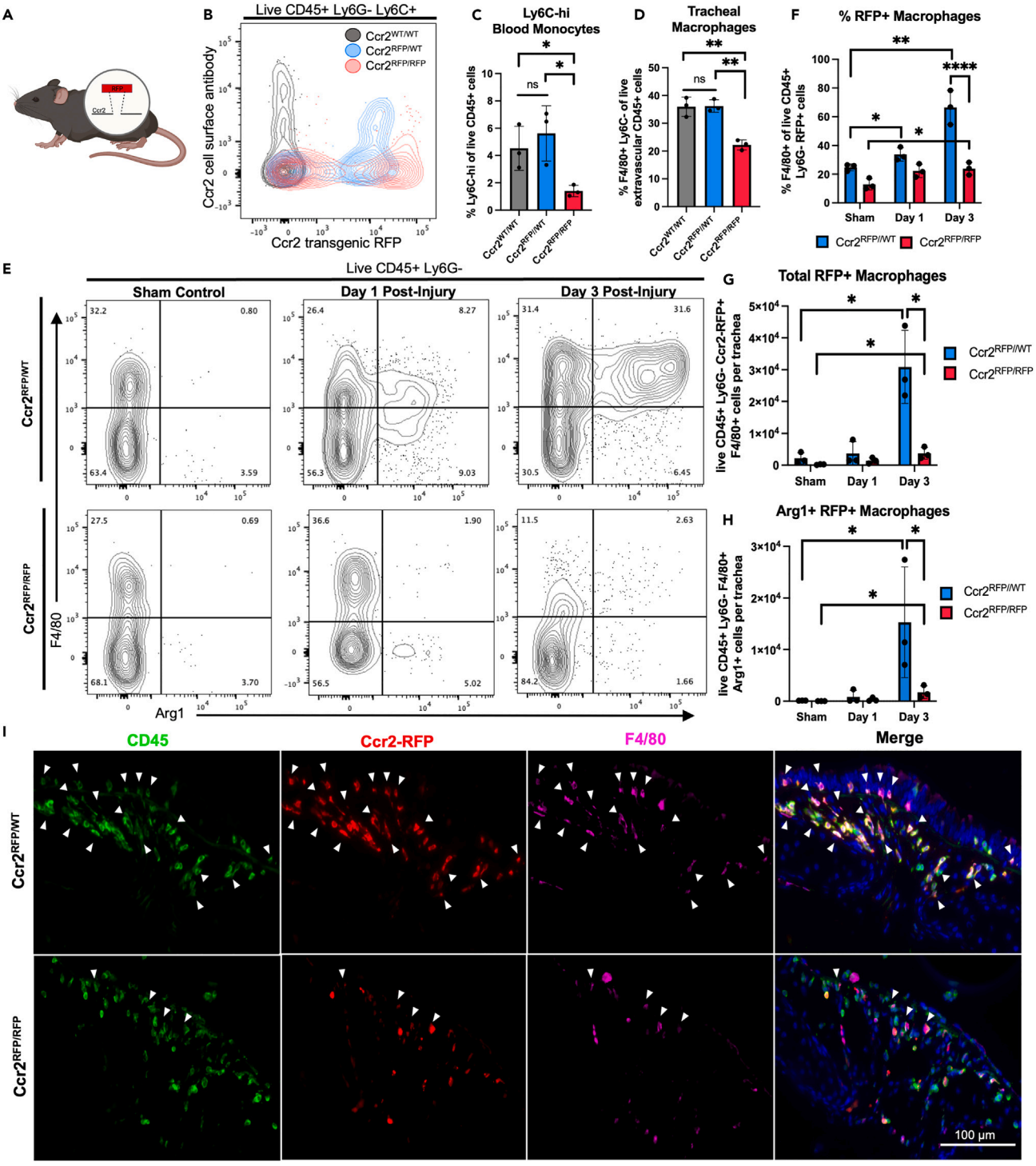

Figure 6. CCR2-deficient mice have reduced monocyte recruitment and impaired macrophage differentiation following tracheal injury

(A) *RFP* is knocked into the endogenous *Ccr2* locus in one (*Ccr2*$^{RFP/WT}$) or both (*Ccr2*$^{RFP/RFP}$) alleles, interfering with expression of functional CCR2 protein.

(B) *Ccr2*$^{RFP/RFP}$ mice show expression of the *Ccr2*-RFP reporter but lack CCR2 cell surface antibody staining by flow cytometry. *Ccr2*$^{RFP/WT}$ animals express both the reporter and the cell surface protein.

(C and D) Quantification of baseline proportions of Ly6C^{hi} circulating monocytes (C) and tracheal macrophages (D) in *Ccr2*$^{RFP/RFP}$ mice compared to WT and heterozygous controls (all groups $n = 3$). Data are presented as mean ± SD.

(E) Flow cytometry showing post-injury macrophage expansion and activation (Arg1^{+}) in *Ccr2*$^{RFP/WT}$ and *Ccr2*$^{RFP/RFP}$ animals.

Figure 6. *Continued*

(F) Proportion of RFP$^+$ cells expressing the mature macrophage marker F4/80 after injury (all groups: $n = 3$). Data are presented as mean ± SD.

(G and H) Quantification of total RFP$^+$ macrophage depletion (G) and Arg1$^+$ macrophage activation (H) in *Ccr2*$^{RFP/RFP}$ mice compared to heterozygous controls (all groups: $n = 3$). Data are presented as mean ± SD.

(I) Representative IF of day 3 post-injury tracheal epithelium showing reduced numbers of CD45$^+$ *Ccr2*-RFP$^+$ F4/80$^+$ cells (arrows) in CCR2-deficient animals compared to heterozygous controls ($n = 3$ per group). (Scale: 100 μm).

*$p < 0.05$, **$p < 0.01$, ***$p < 0.001$, ****$p < 0.0001$.

in response to tracheal injury, there is likely some compensatory proliferation of local tissue-resident macrophages and/or recruitment of monocyte-derived macrophages in a CCR2-independent manner in animals that lack functional CCR2.

CCR2-deficient mice have defective epithelial repair, altered basal cell expansion, and abnormal epithelial morphology following airway injury

To determine whether CCR2-mediated recruitment and activation of monocyte-derived macrophages is required for airway epithelial regeneration and repair, we performed immunofluorescence microscopy to visualize epithelial subpopulations. Both heterozygous and homozygous animals displayed normal pseudostratified epithelial morphology at baseline, with basal cells (NGFR$^+$) lining the epithelial basement membrane and multi-ciliated (aTUB$^+$) and secretory cells (CC10$^+$) comprising the majority of mature epithelial cells lining the airway lumen. Following airway injury and depletion of luminal cells, heterozygote controls displayed normal expansion and stratification of basal cells 3 days after injury, and regeneration of mature secretory and ciliated cells by 7 days post-injury. However, in *Ccr2*$^{RFP/RFP}$ mice, we did not observe normal expansion and stratification of the basal cell population by 3 days post-injury and these mice failed to regenerate mature multi-ciliated cells by 7 days post-injury (Figure 7A). While the regenerated epithelium in control animals returned to a largely non-proliferative quiescent state 7 days post-injury, we observed delayed expansion of basal cells in *Ccr2*$^{RFP/RFP}$ animals at this time point by immunofluorescence imaging and flow cytometry (Figures 7B–7E). Notably, basal cells (KRT5$^+$) in CCR2-deficient animals showed delayed stratification and persistent Ki67 staining 7 days post-injury (Figure 7B). We also observed a significant increase in the percent and total number of proliferating tracheal epithelial cells (EpCAM$^+$ CD45$^-$ EdU$^+$) 7 days after injury by flow cytometry (Figures 7C–7E). Proliferating regions of airway epithelium in CCR2-deficient animals also displayed abnormal epithelial morphology, with elongated KRT5$^+$ CC10$^+$ cells. These elongated cells had apically located nuclei, including Ki67$^+$ nuclei, which may indicate disrupted apical-basal polarity during proliferation (Figure 7B).

While there is a clear delay in epithelial repair in CCR2-deficient animals, the airway appeared morphologically recovered by 21 days post-injury (Figures 7A and 7B), similar to the timeline of repair that has been previously observed in severely immunodeficient NOG animals.[15] By 14 days post-injury, the tracheal epithelium in *Ccr2*$^{RFP/RFP}$ animals contained regions that appear fully regenerated with mature aTUB$^+$ multi-ciliated cells that were interspersed with regions that lacked aTUB and displayed some basal cell stratification, suggesting these regions were not fully differentiated (Figure 7A). We also observed Ki67 labeling in basal cells in these regions of the tracheal epithelium that were not fully regenerated 14 days after injury, suggesting basal cells are still in the process of proliferating and differentiating at this time point (Figure 7B). By 21 days post-injury, CCR2-deficient animals showed consistent aTUB$^+$ labeling throughout the tracheal epithelium, suggesting the epithelium is largely regenerated at this time point (Figure 7A). Small clusters of Ki67$^+$ basal cells can still be observed 21 days post-injury, though the epithelial morphology resembles sham controls. This is similar to what is observed in *Ccr2*$^{WT/RFP}$ controls 14 days post-injury. While there is a significant reduction in Arg1$^+$ macrophage activation in CCR2-deficient animals, this limited macrophage activation likely explains the delay, but not absence of repair in these animals. Future studies could further characterize the contribution of local proliferating tissue-resident airway macrophages to better understand the regenerative potential of pulmonary macrophage subsets and the importance of chemokine receptor-mediated macrophage activation.

Together these data suggest that CCR2 is required for normal recruitment and activation of tracheal macrophages in response to epithelial injury. CCR2-dependent macrophage activation is required for normal epithelial injury response and efficient regeneration of the airway epithelium. The altered immune microenvironment in CCR2-deficient animals may lead to changes in epithelial structural and adhesion components as well as critical signaling pathways that result in defective epithelial proliferation and differentiation.

DISCUSSION

The work presented herein characterizes tracheal macrophages as having a unique phenotypic signature (CD206^{hi} MHC-II^{hi} LYVE-1^{hi} CX3CR1^{hi} CD36^{hi} CCR2^{hi}) that points to a specialized function in the proximal airways. Functional studies demonstrate that tracheal macrophages are critical for normal tissue maintenance/repair and these cells are also able to engage in immune surveillance and pathogen clearance. While these functional characteristics are not unique to macrophages in the proximal conducting airways, these functions are normally performed by specialized, anatomically distinct populations in the distal lung. Tracheal macrophages appear to share features of CD206^{hi}/MHC-II^{lo} peribronchial IMs that are localized along conducting airways and express high levels of scavenger receptors and lysosomal markers and are thought to be critical for homeostatic tissue maintenance.[6] We also demonstrated that tracheal macrophages have high levels of MHC-II and upregulate inflammatory processes following phagocytosis of bacterial bioparticles. It is possible that tracheal macrophages are developmentally similar to CD206^{hi}/MHC-II^{lo} IMs in the distal lung, but by virtue of their higher position in the respiratory tract and increased exposure to environmental stressors and pathogens, these tracheal macrophages become adapted to present antigen and participate in immune surveillance, in addition to their normal homeostatic maintenance functions. Future work could examine tracheal macrophages in pre-/post-natal airways to determine if tracheal macrophages more closely resemble distal lung peribronchial IMs earlier in development.

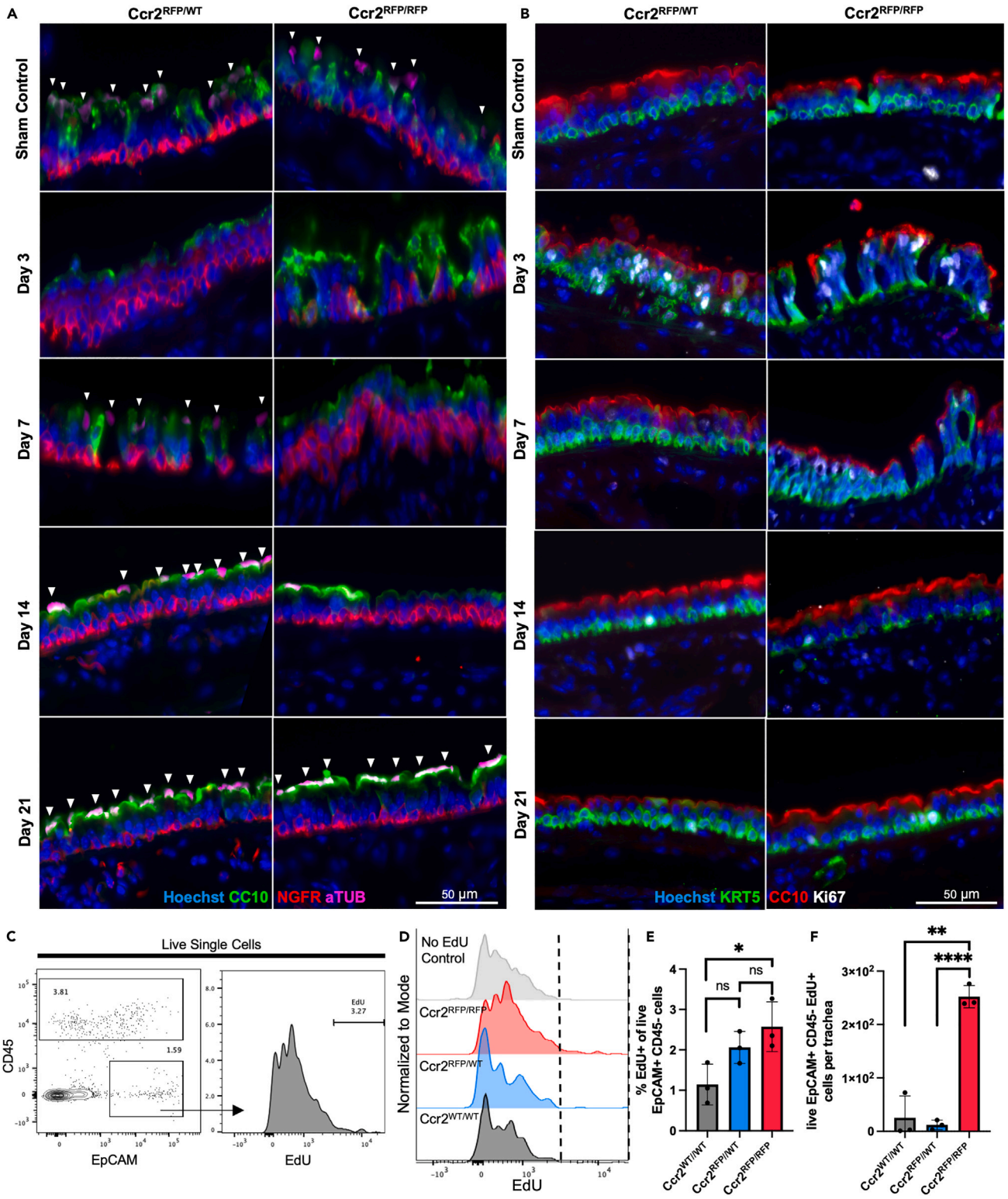
A
Ccr2RFP/WT
Ccr2RFP/RFP
Sham Control
Day 3
Day 7
Day 14
Day 21
Hoechst CC10 NGFR aTUB
50 μm
B
Ccr2RFP/WT
Ccr2RFP/RFP
Sham Control
Day 3
Day 7
Day 14
Day 21
Hoechst KRT5 CC10 Ki67
50 μm
C
Live Single Cells
CD45
EpCAM
3.81
1.59
EdU
EdU
3.27
D
No EdU Control
Ccr2RFP/RFP
Ccr2RFP/WT
Ccr2WT/WT
Normalized to Mode
EdU
E
% EdU+ of live EpCAM+ CD45- cells
*
ns
ns
Ccr2WT/WT
Ccr2RFP/WT
Ccr2RFP/RFP
F
live EpCAM+ CD45- EdU+ cells per trachea
**
****
3×10²
2×10²
1×10²
0
Ccr2WT/WT
Ccr2RFP/WT
Ccr2RFP/RFP

Figure 7. CCR2-deficient mice have defective epithelial repair, altered basal cell proliferation, and abnormal epithelial morphology following airway injury

(A) Representative IF of tracheal epithelium in control and injured airways in CCR2-deficient and heterozygous control animals (all groups: $n = 3$). Mice that lack functional CCR2 show decreased basal cell ($NGFR^+$) expansion, abnormal morphology, and absence of mature multi-ciliated cells ($aTUB^+$) by 7 days post-injury. (Scale: 50 μm).

(B) Representative IF showing altered proliferation ($Ki67^+$) in basal cells ($KRT5^+$) and secretory cells ($CC10^+$) and abnormal epithelial morphology in *Ccr2*$^{RFP/RFP}$ animals (all groups: $n = 3$). (Scale: 50 μm).

(C) Gating strategy for flow cytometric quantification of tracheal epithelial cell proliferation.

(D) Histogram overlays of EdU labeling in epithelial cells ($EpCAM^+$ $CD45^-$) in *Ccr2*$^{RFP/RFP}$ animals 7 days post-injury relative to WT and heterozygous controls (EdU+ gate indicated by the dotted lines).

(E and F) Flow cytometric quantification of percent (E) and total (F) proliferating epithelial cells 7 days post-injury showing delayed basal cell injury response (all groups: $n = 3$). Data are presented as mean ± SD. *$p < 0.05$, **$p < 0.01$, ***$p < 0.001$, ****$p < 0.0001$.

Another important difference between tracheal macrophages and $CD206^{hi}$ peribronchial IMs is their hematopoietic origin. Fate mapping experiments and quantification of proliferation markers revealed that $CD206^{hi}$ peribronchial IMs have increased capacity for self-renewal relative to $CD206^{lo}$ alveolar-associated IMs, with $CD206^{hi}$ peribronchial IMs persisting for approximately one year.[6] In contrast, tracheal macrophages appear to be largely monocyte-derived via Flk2-dependent hematopoiesis, both at homeostasis and following airway injury. Increased immune surveillance pressures in the trachea relative to the distal lung may explain the lack of proliferation and self-renewal in tracheal macrophages and highlights the importance of hematopoietic niches to maintain this population. Similar monocyte-derived macrophage features are observed in the human trachea, suggesting this tracheal macrophage population is relevant in human airway biology and disease.

While the vast majority of Flk2-dependent adult hematopoiesis occurs in the bone marrow, there is increasing evidence that peripheral sites of hematopoiesis exist outside the bone marrow. Hemogenic endothelial cells have been identified in the murine and human fetal lung and have the capacity to undergo endothelial to hematopoietic transition and give rise to hematopoietic progenitors.[44] Future work could more closely examine the route and mechanisms of monocyte development and trafficking to the proximal airways to determine if a pulmonary hematopoietic niche supports and maintains the proximal airway immune microenvironment.

Consistent with previous reports, we observed a significant depletion of circulating $Ly6C^{hi}$ blood monocytes in $Ccr2^{RFP/RFP}$ animals. While CCR2 is the primary chemokine receptor facilitating monocyte egress from bone marrow, it is not strictly required and other chemokine receptors including CX3CR1 and CCR5 can be utilized in the absence of CCR2 to migrate to peripheral tissues.[36–40] While CCR2 is required for efficient repair of the tracheal epithelium, alternative mechanisms may be utilized to repair the airway in a delayed time course. As previously mentioned, local proliferating tissue-resident macrophages may activate an $Arg1^+$ pro-regenerative program in a reduced capacity after injury. Since these animals have dysfunctional monocyte-trafficking and macrophage maturation, it is possible that macrophages in CCR2-deficient animals have a different developmental ontogeny from fully immunocompetent animals and retain a larger proportion of embryonic-derived macrophages in the adult trachea. Future studies could investigate the kinetics of macrophage development in WT and CCR2-deficient animals to determine the regenerative potential of embryonic versus adult hematopoietic macrophages.

Finally, recruitment of monocyte-derived macrophages to the lung in response to injury and persistence of these cells following the resolution of injury is often associated with disease pathogenesis.[45–48] However, other studies have shown that monocyte-derived macrophages limit damaging inflammation and promote the resolution of lung injury.[49,50] Here, we have demonstrated that monocyte-derived tracheal macrophages have a remarkable ability to efficiently activate anti-inflammatory pro-regenerative transcriptional programs, upregulating the activation marker Arg1 and expressing growth factors, matrix enzymes, and chemokines associated with resolution of inflammation and injury. These cells appear to be able to adopt this pro-regenerative phenotype before expressing mature macrophage markers including F4/80 while still in a relatively immature monocyte-like cell state. Understanding the mechanisms that govern monocyte-derived macrophage activation to an anti-inflammatory versus pro-inflammatory state has important implications for understanding human disease pathogenesis and the ability to develop immunomodulatory therapies for human airway disease.

Limitations of the study

These studies characterize tracheal macrophages as specialized airway macrophages that are capable of engaging in both tissue maintenance/repair and immune surveillance. Experiments evaluating the role of tracheal macrophages in airway repair were performed using a sterile tracheal epithelial injury model. Experiments addressing the capacity for tracheal macrophages to respond to pathogens were performed with *ex vivo* using bacterial bioparticles rather than live bacteria. The studies presented herein focused on characterizing the role of tracheal macrophages in airway epithelial injury and regeneration in the absence of an infection and adaptive immune response. *In vivo* infectious injury models were beyond the scope of this manuscript, though further work is needed to characterize the role of tracheal macrophages in immune surveillance, pathogen recognition, and the mechanisms of pro-inflammatory macrophage activation in the proximal extrapulmonary airways.

STAR★METHODS

Detailed methods are provided in the online version of this paper and include the following:

- KEY RESOURCES TABLE

SUPPLEMENTAL INFORMATION

Supplemental information can be found online at https://doi.org/10.1016/j.isci.2024.110169.

ACKNOWLEDGMENTS

We would like to thank the following people for in the BUSM flow cytometry and sequencing cores for their technical assistance: Anna Belkina (BUSM flow cytometry core), Brian Tilton (BUSM flow sytometry core), Dr. Yuriy Alekseyev (BUSM sequencing core), Ashley LeClerc (BUSM sequencing core). This research was funded by the National Institutes of Health grants U01HL134766, F31HL162493, and TL1TR001410.

AUTHOR CONTRIBUTIONS

A.B.Y. and A.E.E. conducted the experiments. P.S.B., F.W., and R.D.C. performed computational analysis. A.B.Y., A.E.E., A.K.Y., J.R.R., J.P.M., and G.J.M. conceived and designed experiments. A.B.Y., A.E.E., and R.D.C. detailed experimental methodologies. A.B.Y. and G.J.M. wrote the manuscript. J.B-E., S.A.M., R.A.F, and J.P.M. provided expertise and feedback.

DECLARATION OF INTERESTS

The authors declare no competing interests.

Received: June 15, 2023
Revised: March 5, 2024
Accepted: May 30, 2024
Published: June 4, 2024

REFERENCES

1. Aegerter, H., Lambrecht, B.N., and Jakubzick, C.V. (2022). Biology of lung macrophages in health and disease. Immunity *55*, 1564–1580. https://doi.org/10.1016/j.immuni.2022.08.010.
2. Gessain, G., Blériot, C., and Ginhoux, F. (2020). Non-genetic Heterogeneity of Macrophages in Diseases—A Medical Perspective. Front. Cell Dev. Biol. *8*, 613116. https://doi.org/10.3389/fcell.2020.613116.
3. Bain, C.C., and MacDonald, A.S. (2022). The impact of the lung environment on macrophage development, activation and function: diversity in the face of adversity. Mucosal Immunol. *15*, 223–234. https://doi.org/10.1038/s41385-021-00480-w.
4. Schneider, C., Nobs, S.P., Heer, A.K., Kurrer, M., Klinke, G., van Rooijen, N., Vogel, J., and Kopf, M. (2014). Alveolar Macrophages Are Essential for Protection from Respiratory Failure and Associated Morbidity following Influenza Virus Infection. PLoS Pathog. *10*, e1004053. https://doi.org/10.1371/journal.ppat.1004053.
5. Chakarov, S., Lim, H.Y., Tan, L., Lim, S.Y., See, P., Lum, J., Zhang, X.-M., Foo, S., Nakamizo, S., Duan, K., et al. (2019). Two distinct interstitial macrophage populations coexist across tissues in specific subtissular niches. Science *363*, eaau0964. https://doi.org/10.1126/science.aau0964.
6. Schyns, J., Bai, Q., Ruscitti, C., Radermecker, C., De Schepper, S., Chakarov, S., Farnir, F., Pirottin, D., Ginhoux, F., Boeckxstaens, G., et al. (2019). Non-classical tissue monocytes and two functionally distinct populations of interstitial macrophages populate the mouse lung. Nat. Commun. *10*, 3964. https://doi.org/10.1038/s41467-019-11843-0.
7. Arafa, E.I., Shenoy, A.T., Barker, K.A., Etesami, N.S., Martin, I.M., Lyon De Ana, C., Na, E., Odom, C.V., Goltry, W.N., Korkmaz, F.T., et al. (2022). Recruitment and training of alveolar macrophages after pneumococcal pneumonia. JCI Insight *7*, e150239. https://doi.org/10.1172/jci.insight.150239.
8. Guillon, A., Arafa, E.I., Barker, K.A., Belkina, A.C., Martin, I., Shenoy, A.T., Wooten, A.K., Lyon De Ana, C., Dai, A., Labadorf, A., et al. (2020). Pneumonia recovery reprograms the alveolar macrophage pool. JCI Insight *5*, e133042. https://doi.org/10.1172/jci.insight.133042.
9. Ricketts, T.D., Prieto-Dominguez, N., Gowda, P.S., and Ubil, E. (2021). Mechanisms of Macrophage Plasticity in the Tumor Environment: Manipulating Activation State to Improve Outcomes. Front. Immunol. *12*, 642285. https://doi.org/10.3389/fimmu.2021.642285.
10. Shapouri-Moghaddam, A., Mohammadian, S., Vazini, H., Taghadosi, M., Esmaeili, S.-A., Mardani, F., Seifi, B., Mohammadi, A., Afshari, J.T., and Sahebkar, A. (2018). Macrophage plasticity, polarization, and function in health and disease. J. Cell. Physiol. *233*, 6425–6440. https://doi.org/10.1002/jcp.26429.
11. Ahamada, M.M., Jia, Y., and Wu, X. (2021). Macrophage Polarization and Plasticity in Systemic Lupus Erythematosus. Front. Immunol. *12*, 734008.
12. Belchamber, K.B.R., and Donnelly, L.E. (2017). Macrophage Dysfunction in Respiratory Disease. In Macrophages: Origin, Functions

and Biointervention Results and Problems in Cell Differentiation, M. Kloc, ed. (Springer International Publishing), pp. 299–313. https://doi.org/10.1007/978-3-319-54090-0_12.

13. Henson, P.M., and Tuder, R.M. (2008). Apoptosis in the lung: induction, clearance and detection. Am. J. Physiol. Lung Cell Mol. Physiol. *294*, L601–L611. https://doi.org/10.1152/ajplung.00320.2007.
14. Han, M.K., Huang, Y.J., LiPuma, J.J., Boushey, H.A., Boucher, R.C., Cookson, W.O., Curtis, J.L., Erb-Downward, J., Lynch, S.V., Sethi, S., et al. (2012). Significance of the microbiome in obstructive lung disease. Thorax *67*, 456–463. https://doi.org/10.1136/thoraxjnl-2011-201183.
15. Engler, A.E., Ysasi, A.B., Pihl, R.M.F., Villacorta-Martin, C., Heston, H.M., Richardson, H.M.K., Thapa, B.R., Moniz, N.R., Belkina, A.C., Mazzilli, S.A., and Rock, J.R. (2020). Airway-Associated Macrophages in Homeostasis and Repair. Cell Rep. *33*, 108553. https://doi.org/10.1016/j.celrep.2020.108553.
16. Basil, M.C., Katzen, J., Engler, A.E., Guo, M., Herriges, M.J., Kathiriya, J.J., Windmueller, R., Ysasi, A.B., Zacharias, W.J., Chapman, H.A., et al. (2020). The Cellular and Physiological Basis for Lung Repair and Regeneration: Past, Present, and Future. Cell Stem Cell *26*, 482–502. https://doi.org/10.1016/j.stem.2020.03.009.
17. Luster, A.D., Weinshank, R.L., Feinman, R., and Ravetch, J.V. (1988). Molecular and biochemical characterization of a novel gamma-interferon-inducible protein. J. Biol. Chem. *263*, 12036–12043. https://doi.org/10.1016/S0021-9258(18)37889-X.
18. Fabriek, B.O., Dijkstra, C.D., and van den Berg, T.K. (2005). The macrophage scavenger receptor CD163. Immunobiology *210*, 153–160. https://doi.org/10.1016/j.imbio.2005.05.010.
19. Abebayehu, D., Spence, A., Boyan, B.D., Schwartz, Z., Ryan, J.J., and McClure, M.J. (2017). Galectin-1 Promotes an M2 Macrophage Response to Polydioxanone Scaffolds. J. Biomed. Mater. Res. *105*, 2562–2571. https://doi.org/10.1002/jbm.a.36113.
20. Yaseen, H., Butenko, S., Polishuk-Zotkin, I., Schif-Zuck, S., Pérez-Sáez, J.M., Rabinovich, G.A., and Ariel, A. (2020). Galectin-1 Facilitates Macrophage Reprogramming and Resolution of Inflammation Through IFN-β. Front. Pharmacol. *11*, 901.
21. de Morrée, A., Flix, B., Bagaric, I., Wang, J., van den Boogaard, M., Grand Moursel, L., Frants, R.R., Illa, I., Gallardo, E., Toes, R., and van der Maarel, S.M. (2013). Dysferlin Regulates Cell Adhesion in Human Monocytes. J. Biol. Chem. *288*, 14147–14157. https://doi.org/10.1074/jbc.M112.448589.
22. Tantawy, M.A., Hatesuer, B., Wilk, E., Dengler, L., Kasnitz, N., Weiß, S., and Schughart, K. (2014). The Interferon-Induced Gene Ifi27l2a is Active in Lung Macrophages and Lymphocytes After Influenza A Infection but Deletion of Ifi27l2a in Mice Does Not Increase Susceptibility to Infection. PLoS One *9*, e106392. https://doi.org/10.1371/journal.pone.0106392.
23. van der Touw, W., Chen, H.-M., Pan, P.-Y., and Chen, S.-H. (2017). LILRB receptor-mediated regulation of myeloid cell maturation and function. Cancer Immunol. Immunother. *66*, 1079–1087. https://doi.org/10.1007/s00262-017-2023-x.
24. Jian, J., Konopka, J., and Liu, C. (2013). Insights into the role of progranulin in immunity, infection, and inflammation. J. Leukoc. Biol. *93*, 199–208. https://doi.org/10.1189/jlb.0812429.
25. Gibbings, S.L., Thomas, S.M., Atif, S.M., McCubbrey, A.L., Desch, A.N., Danhorn, T., Leach, S.M., Bratton, D.L., Henson, P.M., Janssen, W.J., and Jakubzick, C.V. (2017). Three Unique Interstitial Macrophages in the Murine Lung at Steady State. Am. J. Respir. Cell Mol. Biol. *57*, 66–76. https://doi.org/10.1165/rcmb.2016-0361OC.
26. Marriott, H.M., Hellewell, P.G., Cross, S.S., Ince, P.G., Whyte, M.K.B., and Dockrell, D.H. (2006). Decreased alveolar macrophage apoptosis is associated with increased pulmonary inflammation in a murine model of pneumococcal pneumonia. J. Immunol. *177*, 6480–6488. https://doi.org/10.4049/jimmunol.177.9.6480.
27. Tan, S.Y.S., and Krasnow, M.A. (2016). Developmental origin of lung macrophage diversity. Development *143*, 1318–1327. https://doi.org/10.1242/dev.129122.
28. Boyer, S.W., Schroeder, A.V., Smith-Berdan, S., and Forsberg, E.C. (2011). All hematopoietic cells develop from hematopoietic stem cells through Flk2/Flt3-positive progenitor cells. Cell Stem Cell *9*, 64–73. https://doi.org/10.1016/j.stem.2011.04.021.
29. Madissoon, E., Oliver, A.J., Kleshchevnikov, V., Wilbrey-Clark, A., Polanski, K., Richoz, N., Ribeiro Orsi, A., Mamanova, L., Bolt, L., Elmentaite, R., et al. (2023). A spatially resolved atlas of the human lung characterizes a gland-associated immune niche. Nat. Genet. *55*, 66–77. https://doi.org/10.1038/s41588-022-01243-4.
30. Pierce, J.H., Di Marco, E., Cox, G.W., Lombardi, D., Ruggiero, M., Varesio, L., Wang, L.M., Choudhury, G.G., Sakaguchi, A.Y., and Di Fiore, P.P. (1990). Macrophage-colony-stimulating factor (CSF-1) induces proliferation, chemotaxis, and reversible monocytic differentiation in myeloid progenitor cells transfected with the human c-fms/CSF-1 receptor cDNA. Proc. Natl. Acad. Sci. USA *87*, 5613–5617.
31. Pixley, F.J. (2012). Macrophage Migration and Its Regulation by CSF-1. Int. J. Cell Biol. *2012*, 501962. https://doi.org/10.1155/2012/501962.
32. Schioppa, T., Sozio, F., Barbazza, I., Scutera, S., Bosisio, D., Sozzani, S., and Del Prete, A. (2020). Molecular Basis for CCRL2 Regulation of Leukocyte Migration. Front. Cell Dev. Biol. *8*, 615031. https://doi.org/10.3389/fcell.2020.615031.
33. Werner, S., and Grose, R. (2003). Regulation of Wound Healing by Growth Factors and Cytokines. Physiol. Rev. *83*, 835–870. https://doi.org/10.1152/physrev.2003.83.3.835.
34. Ridiandries, A., Tan, J.T.M., and Bursill, C.A. (2018). The Role of Chemokines in Wound Healing. Int. J. Mol. Sci. *19*, 3217. https://doi.org/10.3390/ijms19103217.
35. Stakenborg, M., Abdurahiman, S., De Simone, V., Goverse, G., Stakenborg, N., van Baarle, L., Wu, Q., Pirottin, D., Kim, J.-S., Chappell-Maor, L., et al. (2022). Enteric glial cells favor accumulation of anti-inflammatory macrophages during the resolution of muscularis inflammation. Mucosal Immunol. *15*, 1296–1308. https://doi.org/10.1038/s41385-022-00563-2.
36. Saederup, N., Cardona, A.E., Croft, K., Mizutani, M., Cotleur, A.C., Tsou, C.-L., Ransohoff, R.M., and Charo, I.F. (2010). Selective Chemokine Receptor Usage by Central Nervous System Myeloid Cells in CCR2-Red Fluorescent Protein Knock-In Mice. PLoS One *5*, e13693. https://doi.org/10.1371/journal.pone.0013693.
37. Kuziel, W.A., Morgan, S.J., Dawson, T.C., Griffin, S., Smithies, O., Ley, K., and Maeda, N. (1997). Severe reduction in leukocyte adhesion and monocyte extravasation in mice deficient in CC chemokine receptor 2. Proc. Natl. Acad. Sci. USA *94*, 12053–12058.
38. Boring, L., Gosling, J., Chensue, S.W., Kunkel, S.L., Farese, R.V., Broxmeyer, H.E., and Charo, I.F. (1997). Impaired monocyte migration and reduced type 1 (Th1) cytokine responses in C-C chemokine receptor 2 knockout mice. J. Clin. Invest. *100*, 2552–2561.
39. Serbina, N.V., and Pamer, E.G. (2006). Monocyte emigration from bone marrow during bacterial infection requires signals mediated by chemokine receptor CCR2. Nat. Immunol. *7*, 311–317. https://doi.org/10.1038/ni1309.
40. Tsou, C.-L., Peters, W., Si, Y., Slaymaker, S., Aslanian, A.M., Weisberg, S.P., Mack, M., and Charo, I.F. (2007). Critical roles for CCR2 and MCP-3 in monocyte mobilization from bone marrow and recruitment to inflammatory sites. J. Clin. Invest. *117*, 902–909. https://doi.org/10.1172/JCI29919.
41. Winkler, C.W., Woods, T.A., Robertson, S.J., McNally, K.L., Carmody, A.B., Best, S.M., and Peterson, K.E. (2018). Cutting Edge: CCR2 Is Not Required for Ly6C^{hi} Monocyte Egress from the Bone Marrow but Is Necessary for Migration within the Brain in La Crosse Virus Encephalitis. J. Immunol. *200*, 471–476. https://doi.org/10.4049/jimmunol.1701230.
42. Dyer, D.P., Medina-Ruiz, L., Bartolini, R., Schuette, F., Hughes, C.E., Pallas, K., Vidler, F., Macleod, M.K.L., Kelly, C.J., Lee, K.M., et al. (2019). Chemokine Receptor Redundancy and Specificity Are Context Dependent. Immunity *50*, 378–389.e5. https://doi.org/10.1016/j.immuni.2019.01.009.
43. Nahrendorf, M., Swirski, F.K., Aikawa, E., Stangenberg, L., Wurdinger, T., Figueiredo, J.-L., Libby, P., Weissleder, R., and Pittet, M.J. (2007). The healing myocardium sequentially mobilizes two monocyte subsets with divergent and complementary functions. J. Exp. Med. *204*, 3037–3047. https://doi.org/10.1084/jem.20070885.
44. Yeung, A.K., Villacorta-Martin, C., Lindstrom-Vautrin, J., Belkina, A.C., Vanuytsel, K., Dowrey, T.W., Ysasi, A.B., Vrbanac, V., Mostoslavsky, G., Balazs, A.B., et al. (2022). De-Novo Hematopoiesis from the Fetal Lung. Preprint at bioRxiv. https://doi.org/10.1101/2022.02.14.480402.
45. Misharin, A.V., Cuda, C.M., Saber, R., Turner, J.D., Gierut, A.K., Haines, G.K., Berdnikovs, S., Filer, A., Clark, A.R., Buckley, C.D., et al. (2014). Non-classical Ly6C− monocytes drive the development of inflammatory arthritis in mice. Cell Rep. *9*, 591–604. https://doi.org/10.1016/j.celrep.2014.09.032.
46. Misharin, A.V., Morales-Nebreda, L., Reyfman, P.A., Cuda, C.M., Walter, J.M., McQuattie-Pimentel, A.C., Chen, C.-I., Anekalla, K.R., Joshi, N., Williams, K.J.N., et al. (2017). Monocyte-derived alveolar macrophages drive lung fibrosis and persist in the lung over the life span. J. Exp. Med. *214*, 2387–2404. https://doi.org/10.1084/jem.20162152.

47. Bohnacker, S., Hartung, F., Henkel, F., Quaranta, A., Kolmert, J., Priller, A., Ud-Dean, M., Giglberger, J., Kugler, L.M., Pechtold, L., et al. (2022). Correction to: Mild COVID-19 imprints a long-term inflammatory eicosanoid- and chemokine memory in monocyte-derived macrophages. Mucosal Immunol. *15*, 798. https://doi.org/10.1038/s41385-022-00526-7.
48. Doherty, D.E., Hirose, N., Zagarella, L., and Cherniack, R.M. (1992). Prolonged monocyte accumulation in the lung during bleomycin-induced pulmonary fibrosis. A noninvasive assessment of monocyte kinetics by scintigraphy. Lab. Invest. *66*, 231–242.
49. Machiels, B., Dourcy, M., Xiao, X., Javaux, J., Mesnil, C., Sabatel, C., Desmecht, D., Lallemand, F., Martinive, P., Hammad, H., et al. (2017). A gammaherpesvirus provides protection against allergic asthma by inducing the replacement of resident alveolar macrophages with regulatory monocytes. Nat. Immunol. *18*, 1310–1320. https://doi.org/10.1038/ni.3857.
50. Mirchandani, A.S., Jenkins, S.J., Bain, C.C., Sanchez-Garcia, M.A., Lawson, H., Coelho, P., Murphy, F., Griffith, D.M., Zhang, A., Morrison, T., et al. (2022). Hypoxia shapes the immune landscape in lung injury and promotes the persistence of inflammation. Nat. Immunol. *23*, 927–939. https://doi.org/10.1038/s41590-022-01216-z.
51. Borthwick, D.W., Shahbazian, M., Krantz, Q.T., Dorin, J.R., and Randell, S.H. (2001). Evidence for Stem-Cell Niches in the Tracheal Epithelium. Am. J. Respir. Cell Mol. Biol. *24*, 662–670. https://doi.org/10.1165/ajrcmb.24.6.4217.
52. Anderson, K.G., Mayer-Barber, K., Sung, H., Beura, L., James, B.R., Taylor, J.J., Qunaj, L., Griffith, T.S., Vezys, V., Barber, D.L., and Masopust, D. (2014). Intravascular staining for discrimination of vascular and tissue leukocytes. Nat. Protoc. *9*, 209–222. https://doi.org/10.1038/nprot.2014.005.
53. Finak, G., McDavid, A., Yajima, M., Deng, J., Gersuk, V., Shalek, A.K., Slichter, C.K., Miller, H.W., McElrath, M.J., Prlic, M., et al. (2015). MAST: a flexible statistical framework for assessing transcriptional changes and characterizing heterogeneity in single-cell RNA sequencing data. Genome Biol. *16*, 278. https://doi.org/10.1186/s13059-015-0844-5.
54. Ashburner, M., Ball, C.A., Blake, J.A., Botstein, D., Butler, H., Cherry, J.M., Davis, A.P., Dolinski, K., Dwight, S.S., Eppig, J.T., et al. (2000). Gene ontology: tool for the unification of biology. The Gene Ontology Consortium. Nat. Genet. *25*, 25–29. https://doi.org/10.1038/75556.
55. Gene Ontology Consortium, Carbon, S., Douglass, E., Good, B.M., Unni, D.R., Harris, N.L., Mungall, C.J., Basu, S., Chisholm, R.L., Dodson, R.J., et al. (2021). The Gene Ontology resource: enriching a GOld mine. Nucleic Acids Res. *49*, D325–D334. https://doi.org/10.1093/nar/gkaa1113.
56. Korsunsky, I., Millard, N., Fan, J., Slowikowski, K., Zhang, F., Wei, K., Baglaenko, Y., Brenner, M., Loh, P.R., and Raychaudhuri, S. (2019). Fast, sensitive and accurate integration of single-cell data with Harmony. Nat. Methods *16*, 1289–1296. https://doi.org/10.1038/s41592-019-0619-0.
57. Tran, H.T.N., Ang, K.S., Chevrier, M., Zhang, X., Lee, N.Y.S., Goh, M., and Chen, J. (2020). A benchmark of batch-effect correction methods for single-cell RNA sequencing data. Genome Biol. *21*, 12. https://doi.org/10.1186/s13059-019-1850-9.
58. McCarthy, D.J., Campbell, K.R., Lun, A.T.L., and Wills, Q.F. (2017). Scater: pre-processing, quality control, normalization and visualization of single-cell RNA-seq data in R. Bioinformatics *33*, 1179–1186. https://doi.org/10.1093/bioinformatics/btw777.
59. Durinck, S., Moreau, Y., Kasprzyk, A., Davis, S., De Moor, B., Brazma, A., and Huber, W. (2005). BioMart and Bioconductor: a powerful link between biological databases and microarray data analysis. Bioinformatics *21*, 3439–3440. https://doi.org/10.1093/bioinformatics/bti525.
60. Wang, Y., Sarfraz, I., Pervaiz, N., Hong, R., Koga, Y., Akavoor, V., Cao, X., Alabdullatif, S., Zaib, S.A., Wang, Z., et al. (2023). Interactive analysis of single-cell data using flexible workflows with SCTK2. Patterns (N Y) *4*, 100814. https://doi.org/10.1016/j.patter.2023.100814.
61. Frost, H.R. (2020). Variance-adjusted Mahalanobis (VAM): a fast and accurate method for cell-specific gene set scoring. Nucleic Acids Res. *48*, e94. https://doi.org/10.1093/nar/gkaa582.

STAR★METHODS

KEY RESOURCES TABLE

REAGENT or RESOURCE	SOURCE	IDENTIFIER
Antibodies		
Acetylated tubulin (aTUB)	Sigma T7451	RRID: AB_609894
Anti-chicken secondary	Jackson 703-545-155	RRID: AB_2340375
Anti-chicken secondary	Jackson 703-165-155	RRID: AB-2340363
Anti-goat secondary	Jackson 705-605-147	RRID: AB_2340437
Anti-goat secondary	Jackson 705-165-147	RRID: AB_2307351
Anti-goat secondary	Jackson 705-546-147	RRID: AB_2340430
Anti-mouse secondary	Jackson 715-546-151	RRID: AB_2340850
Anti-rabbit secondary	Jackson 711-165-152	RRID: AB_2307443
Anti-rabbit secondary	Jackson 711-605-152	RRID: AB_2492288
Anti-rat secondary	Jackson 712-605-153	RRID: AB_2340694
Arginase-1 (Arg1)	Invitrogen 17-3697-82	RRID: AB_2734835
CC10/Scgb1a1	gift from Barry Strip	RRID: AB_2910611
CCR2	Biolegend 150605	RRID: AB_2571913
CCR2	Biolegend 150628	RRID: AB_2810415
CD11b	Biolegend 101206	RRID: AB_312789
CD11c	Biolegend 117309	RRID: AB_313778
CD14	Biolegend 123329	RRID: AB_2721526
CD163	Biolegend 155306	RRID: AB_2814060
CD169	Biolegend 142403	RRID: AB_10915470
CD206	Biolegend 141717	RRID: AB_2562232
CD206	Biolegend 141720	RRID: AB_2562248
CD36	Biolegend 102605	RRID: AB_389348
CD45	BD Biosciences 564279	RRID: AB_2651134
CD45	Biolegend 103108	RRID: AB_312973
CD45	R&D Systems AF114	RRID: AB_442146
CD45	Biolegend 103116	RRID: AB_312981
CD45.2	BD Biosciences 612778	RRID: AB_2870107
CD64	Biolegend 139306	RRID: AB_11219391
CD68	Biolegend 137013	RRID: AB_10613469
CD80	BD Biosciences 562611	RRID: AB_2737675
CD86	Biolegend 105032	RRID: AB_2650895
CX3CR1	Biolegend 149005	RRID: AB_2564314
EpCAM	Biolegend 118206	RRID: AB_1134172
F4/80	Biolegend 123132	RRID: AB_11203717
F4/80	Biorad MCA497GA	RRID: AB_323806
F4/80	Biolegend 123116	RRID: AB_893481
F4/80	Biolegend 123110	RRID: AB_893486
F4/80	Invitrogen 47-4801-82	RRID: AB_2735036
FOLR2/FRβ	Biolegend 153303	RRID: AB_2721343
Keratin-5 (KRT5)	Covance Prb-160P	RRID: AB_10063444
Keratin-5 (KRT5)	Biolegend 905901	RRID: AB_2565054

(*Continued on next page*)

Continued

REAGENT or RESOURCE	SOURCE	IDENTIFIER
Ki67	Cell Signaling 9129S	RRID: AB_2687446
Ly6C	Biolegend 128025	RRID: AB_10643867
Ly6G	Biolegend 127617	RRID: AB_1877262
Ly6G	Biolegend 127639	RRID: AB_2565880
Ly6G	Biolegend 127624	RRID: AB_10640819
LYVE1	Invitrogen 50-0443-80	RRID: AB_10598060
MERTK	Biolegend 151507	RRID: AB_2650738
MHC-II	BD Biosciences 562928	RRID: AB_2737897
NGFR	Abcam ab8875	RRID: AB_306828
RFP	Rockland 600-901-379	RRID: AB_10704808
RFP	Rockland 600-401-379	RRID: AB_2209751
SiglecF	BD Biosciences 562680	RRID: AB_2687570
Chemical, peptides, and recombinant proteins		
Polidocanol	Sigma Aldrich	88315-100G
Isoflurane	Henry Schein	29405
Normal Donkey Serum	Jackson ImmunoResearch	017-000-121
Bovine Serum Albumin	Fisher Chemical	BP1600-100
Triton X-	Fisher BioReagents	BP151-100
EdU (5-ethynyl-20-deoxyuridine)	Invitrogen	C10340
LiberaseTM	Millipore Sigma	5401127001
OCT Compound	Fisher Healthcare	4585
Paraffin	Fisher Chemical	T565
Xylene	Fisher Chemical	X3S-4
Paraformaldehyde	Fisher Chemical	O4042-500
Antigen Unmasking Solution, Citric Acid Based	Vector Labs	H-3300
Viability Calcein Blue, AM	Invitrogen	C1429
Viability DRAQ7	Abcam	ab109202
Viability Fixable Blue (UV)	Invitrogen	L23105
Viability Fixable e450	Invitrogen	65-0863-14
Viability Hoechst 33342p	Invitrogen	H1399
EdU Click-it detection kit	Invitrogen	C10636
Deposited data		
Single Cell Sequencing Raw Data	NCBI GEO	GSE152501
Re-analysis of Schyns et al. 2019	EMBL-EBI	E-MTAB-7678
Reanalysis of Madisson et al. 2023	ENA	PRJEB52292
Experimental models: Organisms/strains		
Mouse: C57BL/6J	Jackson Laboratory	RRID: IMSR_JAX: 006965
Mouse: Flk2-Cre (Flt3-Cre)	N/A	T. Boehm and C. Bleul (Max Planck, Freiburg, Germany
Mouse: mT/mG	Jackson Laboratory	RRID: IMSR_JAX: 007576
Mouse: B6.129(Cg)-Ccr2tm2.1Ifc/J	Jackson Laboratory	RRID: IMSR_JAX: 017586
Software and algorithms		
Fiji/ImageJ	Fiji	https://fiji.sc/

(*Continued on next page*)

Continued

REAGENT or RESOURCE	SOURCE	IDENTIFIER
NIS-Elements	Nikon	https://www.microscope.healthcare.nikon.com/products/software/nis-elements
FlowJo	BD Biosciences	https://www.flowjo.com/
Cell Ranger	10X Genomics	v.2.0.1
Seurat	Satija Lab	v3
MAST	Finak et al.[53] (2015)	https://github.com/RGLab/MAST
BioMart	Durinck et al.[59] (2005)	https://www.ebi.ac.uk/biomart
VAM (Variance Adjusted Mahalanobis)	Frost et al.[61] (2020)	http://www.dartmouth.edu/~hrfrost/VAM

RESOURCE AVAILABILITY

Lead contact

Further information and requests for resources should be directed to and will be fulfilled by the lead contact, George Murphy (gjmurphy@bu.edu).

Materials availability

This study did not generate new unique reagents.

Data and code availability

The scRNA-seq data is available in the NCBI GEO repository under accession number GSE152501. This paper analyzes existing, publicly available data. The accession numbers for these datasets are listed in the key resources table. Any additional information required to reanalyze the data reported in this paper is available from the lead contact upon request. This paper does not report original code.

EXPERIMENTAL MODEL AND STUDY PARTICIPANT DETAILS

Mice

8-12 week old (C57BL/6J), Flk-Switch[7,28] and *Ccr2*-RFP (B6.129(Cg)-*Ccr2*$^{tm2.1Ifc}$/J)[36] mice were used for monocyte and macrophage studies. All mice were bred and maintained in a specific-pathogen-free barrier facility with free access to food and water. Both male and female mice were used in a sex-unbiased manner for all experiments except for experiments utilizing Flk-Switch mice, which only used male mice because the Flk2-Cre transgene is contained in the Y chromosome. All studies utilized a minimum of three animals per experimental group. All animal housing and experimental procedures were approved by the BUSM IACUC under license PROTO202000057.

METHOD DETAILS

Airway injury

Polidocanol-induced injury was performed as previously described.[15,51] Mice were anesthetized in an Isoflurane chamber and delivered one dose of 20 μL freshly prepared, 2% Polidocanol or PBS sham control by oropharyngeal aspiration to induce injury. Tracheas were harvested 1-, 3- or 7-day following injury for analysis by scRNA-Seq, flow cytometry, or histology/immunofluorescence.

Tissue preparation

Mice were euthanized with a combination of Isoflurane overdose and abdominal aorta exsanguination. The thoracic cavity was opened and the pulmonary vasculature was perfused with PBS via the right heart ventricle before tracheas and/or lungs were dissected under stereomicroscope magnification. Whole tracheas and lung were digested with 1.5 mg/mL Collagenase A (Roche), 0.4 mg/mL DNase I (Roche), and 2 U/mL Dispase (Sigma–Aldrich) in RPMI base medium at 37°C for 30–45 min, or with 0.5 mg/mL Liberase in DMEM base medium at 37°C for 30–45 min. Reaction was stopped using FBS to a concentration of 10% and filtered through 40 μm cell strainers. RBC lysis was performed as needed. For tissue collection for immunohistochemistry, whole throats were dissected and fixed for maximally 4 h in 4% PFA. PFA was washed out of tissue using PBS and the trachea was dissected out of the throat. Tracheas were either embedded in paraffin for histology by moving through ascending ethanol (50%–100%), xylene and paraffin in a vacuum oven and sectioned at 5–7 μm on a microtome (Leica) or were prepared for frozen sectioning, by cryopreservation in 30% sucrose for 48 h, embedding in OCT medium and freezing on dry ice. Frozen organs were sectioned on Cryostat (Leica) at 8–12 μm thickness within one month and sectioned tissue was stored at −20°C. For detection of EdU incorporation in proliferating cells, 200 μL EdU was injected intraperitoneally 3 h prior to tissue harvest.

Flow cytometry

Single cell suspensions of tissue digests (as described in tissue preparation) were kept on ice and stained in flow cytometry/FACS buffer (1% BSA in PBS without Ca^{2+} or Mg^{2+}). For live cell staining and sorting, a cell viability dye (Calcein Blue, DRAQ7, Fixable e450, or Fixable UV Blue) was added before sample acquisition. Flow cytometry analysis was performed on a Stratadigm (S1000EXI), FACSAria II (BD Biosciences), or LSR II (BD Biosciences) and cell sorting was performed on Moflo Astrios (Beckman Coulter). Compensation was performed with single-stained UltraComp compensation beads (Thermo Fisher) or single-stained immune cells prepared from spleen or lung. To determine gating controls for reporter gene expression, mice lacking the reporter or protein were used. Initial data cleanup and expert-driven analysis were performed using FlowJo (BD Biosciences) and Cytobank cloud-based analysis software (Beckman Coulter). For analysis of macrophage origin in Flk-Switch mice, intravascular immune cells were labeled by tail vein injection[52] of 2 μg of CD45-BUV737 (BD Biosciences) diluted in 100 μL of sterile saline and loaded into a 28.5 gauge insulin syringe. For tail vein injection animals were lightly anesthetized, injected and kept under controlled, anesthetized conditions, before right ventricle transcardial perfusion 3 min post-injection. EdU staining was performed using a Click-it EdU detection kit according to manufacturer recommendations.

Tissue histology and immunofluorescence

Paraffin-embedded slides were rehydrated by consecutive, descending processing through xylene and ethanol (100%–50%). Paraffin-preserved and frozen sections underwent citrate-based antigen retrieval prior to blocking and permeabilization for 30–60 min in 10% NDS, 4% BSA and 0.5% Triton X-. Primary antibodies were diluted in primary block solution (2.5% NDS, 1% BSA, 0.125% Triton X-) and incubated for at least 1 h at room temperature or overnight at 4°C in a humidified chamber. All fluorophore-conjugated secondary antibodies were diluted in secondary block solution (5% NDS, 2% BSA, 0.25% TX). Nuclei were labeled using a Hoechst nuclear stain at 1:1000 for 5 min at room temperature.

Single cell RNA sequencing

Tissue was prepared as described above for flow cytometry and FACS. For homeostatic comparison of tracheal and lung macrophage populations, viable $CD45^+$ $F4/80^+$ were sorted from 5 animals per tissue and pooled for sequencing. Tracheal cells were collected separately as intra-epithelial and sub-epithelial samples using light digestion and peeling of the tracheal epithelium prior to bulk digest of the remaining subepithelial tissue. For post-polidocanol injury sequencing we sorted viable bulk $CD45^+$ cells from 3 animals per condition, pooled cells for sequencing for each condition, and limited subsequent analysis to cells expression the macrophage marker *Adgre1*. Cells were brought to appropriate concentration according to 10X protocol recommendation. Single cells were captured for sequencing library preparation using a 10X Chromium (10X Genomics, Pleasanton, CA) instrument at the BUMC Single Cell Core. Library preparation and sequencing was done at the Boston University Division of Computational Biomedicine and Boston University Microarray and Sequencing Resource (BUMSR) Core. Single-cell RNA-seq libraries were prepared according to the Single Cell 3′ v2 Reagent Kits User Guide (10X Genomics). Sequence libraries were constructed using the Chromium Single-Cell 3′ Library Kit (10X Genomics) and loaded on a NextSeq500 (Illumina) to obtain a sequencing depth of~200K reads per cell. 1,050 cells from the trachea and 460 cells from whole lung parenchyma were captured and sequenced. For intra-epithelial trachea, 143,824 mean reads per cell were obtained corresponding to 2,133 UMI counts and 908 genes expressed per cell. For sub-epithelial trachea 190,186 reads per cell were obtained corresponding to 5383 UMI counts and 1,891 genes expressed per cell. For the lung parenchyma, 320,071 mean reads per cell were obtained corresponding to 3,969 UMI counts per cell and 1,636 genes expressed per cell. For post-polidocanol injury experiments 5,307 cells were captured and sequenced, 458 cells from uninjured controls, 1,625 cells from day 1 post-injury, 1,507 from day 4 post-injury, and 1,717 cells from day 7 post-injury. For the control sample, 252,388 reads per cell were obtained corresponding to 14,098 UMI counts per cell and 3,132 genes expressed per cell. For the day 1 sample, 78,790 reads per cell were obtained corresponding to 12,141 UMI counts per cell and 2,834 genes expressed per cell. For the day 4 sample, 97,091 reads per cell were obtained corresponding to 12,598 UMI counts per cell and 2,928 genes expressed per cell. For the day 7 sample, 89,387 reads per cell were obtained corresponding to 12,620 UMI counts per cell and 2,912 genes expressed per cell.

Bioinformatic analysis

Single cell reads were mapped to the mouse genome reference (ENSEMBL, GRCm38) and pre-processed with Cell Ranger v.2.0.1 to obtain the matrix of UMI counts per gene per cell. Seurat v.3 was used to normalize, scale and regress out unwanted sources of variation including cell degradation based on mitochondrial fraction (15% threshold), and subsequently identified highly variable genes for linear dimensionality reduction using PCA. The principal components were then used for event clustering using the Louvain algorithm. Further non-linear dimensionality reduction and visualization was done using UMAP. Differential gene expression was tested using MAST,[53] and clusters identified with the Louvain method were annotated based on their DEGs. To understand the functional implications of DEGs, we utilized the Gene Ontology database to identify gene sets enriched in various cell signaling pathways and biological processes.[54,55] Harmonization of scRNA-seq data from Engler et al. (2020)[15] and Schyns et al. (2019)[6] was performed using the Harmony algorithm which allows for batch-effect correction of different biological and experimental conditions to group cells by type.[56,57] Harmonized scRNA-seq analysis combined sequencing data from the previous section (1,510 cells total) with 4,628 cells from Schyns et al. (2019),[6] including $CD45^+$ $F4/80^+$ $CD64^+$ IMs (2,047 cells), $Ly6C^{hi}$ monocytes (1,575 cells) and $Ly6C^{lo}$ monocytes (1,006 cells). Single-cell RNA-sequencing data of human myeloid cells was obtained from Madissoon et al. 2023 via their cellxgene portal (https://5locationslung.cellgeni.sanger.ac.uk/cellxge ne.html).[29] The myeloid data

was subsetted to the nine unique macrophage populations for the purposes of this analysis, resulting in 28,309 cells total. Log-normalized counts of the provided expression matrix were calculated using scuttle's 'logNormCounts' function with default parameters.[58] Macrophage gene lists ranked by relative expression in murine data were converted to human symbols using BioMart in R.[59] Metagene scores for the top 100 genes in preserved order from the murine gene lists were calculated with VAM (Variance Adjusted Mahalanobis) using the Single Cell Toolkit with default parameters on the log-normalized counts assay.[60,61]

Statistical analysis

Images were analyzed and quantified with ImageJ/FIJI (version 2.9.0, NIH). Statistical significance was determined by ANOVA and two-tailed Student's t test for all group comparisons except for analysis of $Arg1^+$ macrophages, which was determined using one-tailed Student's t tests. Significance was determined as $*p < 0.05$, $**p < 0.01$, and $***p < 0.001$; Deviance from the mean is displayed as standard deviation.